Chemical Engineering Science 280 (2023) 118964

Contents lists available at ScienceDirect

Chemical Engineering Science

journal homepage: www.elsevier.com/locate/ces

A model for the absorption rate in electrically charged droplets

F. Di Natale [a], A. Parisi [a,*], C. Carotenuto [b], A. Lancia [a]

[a] Dipartimento di Ingegneria Chimica, dei Materiali e della Produzione Industriale, Università di Napoli Federico II, Piazzale Tecchio 80, 80125 Napoli, Italy
[b] Dipartimento di Ingegneria, Università della Campania "L. Vanvitelli", Via Roma 29, 81031 Aversa, CE, Italy

ARTICLE INFO

Keywords:
Separation processes
Absorption
Charged droplets
Electrospray
Wet scrubbing

ABSTRACT

Charged droplets are produced by electrosprays or sometimes generated by natural phenomena, and nowadays their application is also investigated as a tool for process intensification in heat and mass transfer processes typical of chemical engineering. This paper analyses the absorption of slightly soluble trace gases into electrically charged droplets: it reports a new mass transfer model taking into account the electrophoretic motion of gas molecules and the possible alteration of the interfacial properties induced by the imposed electric charges. The model is successfully validated against existing experiments on the absorption of SO_2 into electrified water droplets. These experiments are useful both for the robustness of data available for the SO_2-air-water system and for its significance in atmospheric chemistry and physics, and chemical engineering applications.

Considering the same SO_2-air-water system as a case study, the model predicts that the absorption rate for a droplet produced with a conventional electrospray is up to 42% faster than that of an uncharged droplet with the same size and morphology, while the electrophoretic drift provides an improvement of the gas-side mass transfer coefficient mainly for droplets finer than 500 μm.

1. Introduction

Absorption and desorption are among the most important phenomena occurring at a liquid–gas interface. Indeed, they affect the nature of the liquid interfacial composition and determine the partitioning of chemicals in the two phases (Giberti and Hassanali, 2017; Shamay et al., 2011). Absorption and desorption are widely used in chemical processes and pollution control systems (Flagiello et al., 2020; Couper, 2010; Flagiello et al., 2019; Green and Perry, 2018; Jiang et al., 2020; Sharif et al., 2021; Sinnott and Towler, 2019; Valluri and Kawatra, 2021), but are also important for several natural phenomena, influencing, for example, the wet deposition of water-soluble pollutants or the desorption of CO_2 from natural waters (Elhajj et al., 2014; Jain et al., 2019; Yu et al., 2020).

One of the less explored aspects of absorption processes is the effect of free electric charge deposited over the liquid surface although, differently from the common understanding, electrically charged liquids are largely diffused in Nature (Beattie, 2016; Choi et al., 2017; Galembeck and Burgo, 2017; Horikoshi and Serpone, 2017; Pruppacher and Klett, 2010; Tinsley et al., 2006; Tinsley et al., 2000; Vácha et al., 2007) and are intentionally produced in several industrial processes (*e.g.* Borra, 2018; Burgo and Galembeck, 2016; Galembeck and Burgo, 2017; Shrimpton, 2009).

Droplets are among the most common form of charged liquid interfaces used in engineering applications. In this kind of geometry, curvature effects play an important role in the distribution of charge and in the development of interfacial phenomena and chemical reactions (Consta, 2022; Funakawa and Balachandran, 2006; Hassan et al., 2021; Kwan and Consta, 2021, 2020; Malevanets and Consta, 2013; Reznikov et al., 2003; Salazar et al., 2015).

One possible way to generate large amounts of charged droplets is electrospraying or electrohydrodynamic atomization, a process which involves both hydro/aerodynamic forces and electric fields to produce sprays of diminutive droplets. Electrospraying is used in several chemical processes, such as fine and ultrafine particle filtration, solvent extraction, desalination, humidification, surface coating or mass spectroscopy and a far larger number of processes for material science and biomedical applications (Agostinho et al., 2018; Boda et al., 2018; Bodnár et al., 2018; Borra, 2018; Carotenuto et al., 2010; Castillo et al., 2018; Cui et al., 2017; Di Natale et al., 2015; Hu and Yao, 2018; Kim et al., 2020; Kishimoto et al., 2017; Li et al., 2022; Martin et al., 2017; Parmentier et al., 2016; Rosell-Llompart et al., 2018; Sharif et al., 2021).

The absorption of a gas solute into charged drops is studied in a few papers which were recently reviewed by Di Natale and co-workers

* Corresponding author.
E-mail address: arianna.parisi@unina.it (A. Parisi).

https://doi.org/10.1016/j.ces.2023.118964
Received 27 January 2023; Received in revised form 14 May 2023; Accepted 1 June 2023
Available online 6 June 2023

(2020, 2019, 2018). The largest majority of the experimental results, mostly referring to the SO_2-water-air system, agreed that the rate of absorption increases by increasing the droplet's charge density (Byun et al., 1998; Di Natale et al., 2020, 2019, 2018; Dou et al., 2009; Li et al., 2022; Matteson and Giardina, 1974; Wang, 2013). Most of these authors associated this result with the alteration of spray surface area and droplet deformation arising from the electrospray process. However, the sole modification of droplet morphology does not seem sufficient to explain the experimental results. Recent attempts have been made by Di Natale et al. (2019) who, despite the availability of accurate data on droplet morphology, needed additional parameters to account for the role of droplet charge density described in their experiments. Similarly, Li et al. (2022) introduced an empirical enhancement factor to describe their data.

The droplets' charge density is also known to influence several interfacial properties (Burgo and Galembeck, 2016; Conde et al., 2021; Galembeck and Burgo, 2017; Kallay et al., 2015; Matteson and Giardina, 1974; Ohshima and Furusawa, 1998; Ovchinnikova and Pollack, 2009; Santos et al., 2011; Wei et al., 2018). Matteson and Giardina (1974) successfully linking the absorption rate of SO_2 on charged droplets to a higher interfacial solubility deriving from the lower interfacial tension of charged droplets. More recent papers reported an alteration of the molecular composition at the interface and a different distribution of interfacial OH^- and H_3O^+ ions during the water charging process (Burgo and Galembeck, 2016; Malevanets and Consta, 2013; Ovchinnikova and Pollack, 2009; Santos et al., 2011; Wei et al., 2018). Recently, Consta (2022) showed the correlation between the onset of local Rayleigh fission instabilities and ions ejection, *i.e.* a desorption process. Classical interfacial thermodynamics also indicated differences in the chemical potential of charged water droplets, that explains the condensation of moisture on charged jets and droplets (Reznikov et al., 2003; Salazar et al., 2015). A detailed presentation of these works is outside the scope of this paper, but the general conclusions that can be gathered from them are that the equilibrium conditions for a solute on a charged surface are likely to be different from those holding for an uncharged one, and these differences are not only related to the curvature of the surface, but also to specific alteration of the molecular structure of charged droplet.

Finally, the occurrence of electrodynamics interactions among charged droplets and dipolar molecules, such as SO_2, is likely to take place (Uchigasaki et al., 1967; Wang and Luo, 2011). Wang and Luo (2011) proposed the introduction of an additional electrophoretic flow to incorporate droplet charge effects in the absorption rate calculation. Although conceptually understandable, the paper was later retired probably because of some errors in the mathematical formulation of the proposed model.

The analysis of the pertinent literature thus reveals that a definite model for the absorption rate of charged droplets is still far to come.

This paper proposes a new model to describe the absorption of a dilute gas solute (*e.g.* a trace gas pollutant, such as SO_2 or NO_x) into charged water droplets, by including all the main features of literature models. Indeed, the model is based on:

i) The availability of data on droplets size and morphology, which permits the selection of more suitable state-of-the-art models for the absorption of dilute solutes into spherical and deformed droplets;
ii) The adoption of a semi-empirical model to correlate the interfacial solubility and the droplet charge density.
iii) The inclusion of the electrophoretic flow of dipolar molecules toward charged drops.

The paper is divided into three main sections. In the first section, the model is presented. Then, the model is validated using a set of experiments reported by our research group in a former paper (Di Natale et al., 2020) and is critically explored to better understand how droplet morphology, interfacial solubility and electrophoretic transportation impact the model's ability to describe the experimental data. Finally, in the third section, the effect of three main process parameters, droplet charge density, droplet diameter and interfacial solubility is studied, so to compare the expected absorption rate of charged droplets with the corresponding value for uncharged droplets.

2. Absorption model

In this section, we describe the equations used to predict the absorption rate of a charged droplet exposed to an ideal gas carrier containing small concentrations of a single solute under nearly isothermal conditions and in absence of solvent evaporation, so that a negligible correlation between the extent of absorption and volume of the droplets can be considered. The mass transfer of the gas carrier in the liquid solvent (and *vice versa*) is neglected, as well as the occurrence of chemical reactions in the liquid phase.

In the following section, the adsorption model for an uncharged droplet is first resumed; then, the case of charged droplets is presented.

2.1. Absorption model for uncharged droplets

At the microscopic scale, field equations (mass, momentum and energy balances) should be integrated to determine the time-dependent local mass flux of the solute through the interface of a droplet ($mol \cdot m^{-2} \cdot s^{-1}$). However, this solution can be rigorously addressed only for a simple and well-determined fluid dynamic field, when turbulence inside and outside the droplet is absent.

For many practical applications, the transport of the solute through a droplet is averaged along the surface and an overall mass balance is adopted (*e.g.* Bird et al., 2007; Levenspiel, 1999):

$$\frac{dn}{dt} = \frac{d(x \cdot V_d)}{dt} = N_0 \cdot A \tag{1}$$

Where n (mol) is the total moles of solute in the liquid droplet (*i.e.* the product between the concentration x, in $mol \cdot m^{-3}$, and the droplet volume V_d in m^3), A is the droplet surface (m^2) and N_0 is the surface average mass flux in ($mol \cdot m^{-2} \cdot s^{-1}$). In the following, the concentration in the gas phase is indicated as y ($mol \cdot m^{-3}$). The mass flux originates from gradients in the chemical potentials of the species between the two sides of the gas–liquid interfaces.

The most common approach to describe the mass flux at a gas–liquid interface is the classical two-films theory (Whitman, 1962) which assumes the transport phenomena to occur into two boundary layers (the gas and the liquid films) surrounding the interface. A detailed description of the theory and its application to absorbers design can be found in several reference textbooks (*e.g.* Bird et al., 2007; Sinnott and Towler, 2019; Zarzycki and Chacuk, 1993). The two-film theory assumes that the heat, momentum and mass fluxes through the interface are so fast that equilibrium conditions hold: the liquid and gas phases at the two sides of the interface have the same pressure and temperature of the interface (P_I and T_I usually in Pa and K) as well as the same chemical potential. These conditions translate into equilibrium correlations between the liquid and the gas concentration of the solute at the two sides of the interface. For very dilute solutions containing one solute, the equilibrium correlation is well described through a constant partition factor (Henry's law type) equation for interfacial solubility:

$$y_I = m_0 x_I \tag{2}$$

where x_I and y_I are, respectively, the concentration of the solute on the liquid and the gas side of the interface. The constant partition factor, m_0 is a function of temperature, pressure, and liquid and gas overall composition at the interface.

According to the two-films theory, during absorption, the solute is transferred from the gas to the liquid bulk after passing through the

series of two boundary layers regions, one on the gas side and the other one on the liquid side of the interface, where the solute moves under the concentration gradients imposed by the differences (y - y_I) and (x_I - x): The average mass flux, N_0 (mol·m^{-2}·s^{-1}), can be referred to these single-phase boundary layers considering two linear driving forces as:

$$N_0 = k_g \cdot [y - y_I] = k_l \cdot [x_I - x] \tag{3}$$

where k_g and k_l are defined as the mass transfer coefficients in the gas and the liquid films, in (m·s^{-1}).

The mass flux for uncharged droplets is most commonly described as:

$$N_0 = k_g^o \cdot [y - y^*] \tag{4}$$

Where k_g° is the overall mass transfer coefficient for dilute solute transport, and y^* is defined as the concentration of the solute in the gas phase corresponding to the application of the interfacial equilibrium correlation to the solute concentration in the bulk liquid phase, x:

$$y^* = m_0 x \tag{5}$$

From this equation, it is possible to correlate the values of y_I as a function of y and y^* as:

$$y_I = \frac{m_0 k_g y + k_l y^*}{m_0 k_g + k_l} \tag{6}$$

The two-films theory also provides a correlation between mass transfer coefficients. Taking into account the equilibrium conditions held at interfaces, the overall mass transfer coefficient for dilute solute transport is defined as:

$$k_g^o = \left[{k_g}^{-1} + m_0 {k_l}^{-1} \right]^{-1} \tag{7}$$

Probably, the main advantages of the two-film theory are the possibility of decoupling the estimation of k_g and k_l through suitable experiments and the longstanding experience in the development of robust models to describe k_g and k_l for many different fluid dynamic conditions and exchange surface morphologies, also accounting for their dependence on the relevant physical properties of the fluids (*e.g.* density, viscosity, diffusivities, surface tension).

For the case of an isolated droplet immersed in a gas phase, the pertinent literature identified three main fluid dynamic conditions to characterise the gas motion around the droplet (laminar, steady circulating and unsteady oscillating flows), and three for the liquid motion (stagnant, internal circulation and oscillating droplets flow) inside the droplet as a function of droplet size, relative droplet-gas velocity and physical properties of the system at hand (*e.g.* Bhaga and Weber, 1981; Clift et al., 1978; Flagiello et al., 2019; Grace et al., 1976; Green and Perry, 2018; Kumar and Hartland, 1999; Michaelides et al., 2017; Wegener et al., 2014). Each condition is described by a specific class of models and gives rise to different values of the mass transfer coefficients: these are the highest for turbulent flows with oscillating droplets and the smallest for laminar flows with stagnant droplets.

The mass transfer coefficients are a function of: i) the average droplet size (usually expressed as the mean Sauter diameter, d_{32} in m), ii) the physical properties of the gas and the liquid and the solute diffusivities in the gas and the liquid phases, often resumed by the Schmidt number:

$$Sc_p = \frac{\mu_p}{D_p \rho_p} \tag{8}$$

iii) the fluid dynamic field close to the interface, resumed by the average Reynolds number:

$$Re_p = \frac{\rho_p d_{32} U_p}{\mu_p} \tag{9}$$

and iv) the droplet degree of deformation - represented by the ratio between the maximum and the minimum values of the surface area observed for a deformed, oscillating droplet, ($1 + \varepsilon$) – and their frequency of oscillation ω (rad·s^{-1}) (Schroeder and Kintner, 1965). In Eqs. (8)–(9) the suffix p indicates the relative phase, either the gas or the liquid, g or l.

An analysis of the specific correlations between physical parameters and mass transfer coefficients is beyond the scope of this work, but the models predict higher values of k_g and k_l for higher values of the relative gas–liquid velocity (U), the droplet's oscillation frequency and deformation (ω and ε), the diffusivities (D_g and D_l) and for lower values of the liquid viscosity (μ_l). The effects of droplet diameter are more complex to assess because of its repercussions on U, ω and ε.

Finally, as from Eq. (1), the actual amount of solute transferred from one phase to the other also depends on the actual exchange area, *i.e.* on the area of the liquid–gas interface, A (Bird et al., 2007; Sinnott and Towler, 2019; Zarzycki and Chacuk, 1993), and therefore, on the droplet morphology. The main parameters describing this morphology are the average size, d_{32}, the droplet degree of deformation ($1 + \varepsilon$) and the oscillation frequency, ω. Indeed, while the mass and the volume of a droplet are constant, its surface strongly depends on the fluid dynamic conditions (Clift et al., 1978). There are two extreme cases: for low Reynolds number and high surface tension, droplets behave as rigid spheres (ω, $\varepsilon = 0$, A is the area of a sphere of radius d_{32}), while for high Reynolds number and low surface tension, the droplets are largely deformed, and their shape change over time (ω, $\varepsilon > 0$, A is the variable area of an oscillating ellipsoid).

To the authors' experience, droplet morphology and oscillations are the most complex parameters to be predicted and, whenever possible, they should be derived from direct experimental investigations under representative conditions. All the other parameters required for the calculation of k_g and k_l can be retrieved from specialistic literature.

Once the droplet surface area, the interfacial equilibrium conditions and the mass transfer coefficient equations are known, Eq. (1) can be solved to calculate the amount of solute absorbed over time upon exposure to a gas containing the solute at concentration y, after imposing the required initial condition. Usually, the formulation of Eq. (4) referring to the overall mass transfer resistance is adopted but, for the scope of this work, the one referring to the gas phase resistance – Eqs. (3)–(6) – is preferred:

$$\frac{dn}{dt} = k_g^0 A \left[y - m_0 \frac{n}{V_d} \right] = k_g A \left[y - \frac{m_0 k_g y + k_l y^*}{m_0 k_g + k_l} \right] \tag{10}$$

$$t = 0 \quad n = n_0 \tag{11}$$

2.2. Absorption model for charged droplets

The absorption rate of a neutral molecule in charged droplets can be calculated starting from the Eqs. (10)–(11) valid for the uncharged ones.

In this model we consider how the charging process alters the droplet morphology (a phenomenon typical of small-scale electrospray processes but less evident in other situations as shown, for example, by Di Natale et al., 2015; Dou et al., 2009; Krupa et al., 2013; Rosell-Llompart et al., 2018; Wang et al., 2007) because it alters the actual exchange area, the fluid dynamic fields outside and inside the droplets and, implicitly, the mass transfer coefficients in the gas and the liquid films. Besides, we also consider the possible alteration of the interfacial solubility deriving from droplet charge, following the suggestion of Matteson and Giardina (1974) and the electrophoretic interactions as suggested by Wang and Luo (2011).

The proposed model is based on the following assumptions:

1. The effects of electric charge over the diffusivities of species in the liquid phase are neglected - an assumption that may appear valid for ionic liquid as water, whose cations and anions concentration is far larger than the net charge usually imposed over the droplet.

2. The fluid dynamics of the gas and the liquid phase are determined by the droplet size, morphology and deformation but are not directly altered by the presence of the electric charge. Similarly, we assume the equations available for convective/diffusive mass transfer coefficients for the gas and liquid phases are equal to those available for uncharged droplets.
3. Following the approach initially proposed by Wang and Luo (2011), and under the assumption of linear superimposition of mass flows, we considered that, for charged droplets, the electrophoretic and the diffusive/convective mass fluxes in the gas phase are additive.
4. The Marangoni effect induced by gradients in surface tension is neglected.

Under these last assumptions, the mass flux (Eq. (5)) can be expressed as:

$$N = k_g \cdot [y - y_I] + N_e = k_l \cdot [x_I - x] \tag{12}$$

where N_e is the electrophoretic flow, (mol·m^{-2}·s^{-1}).

The electrophoretic contribution derives from the electric forces acting on gas molecules. Such electrophoretic forces are expected to take place either if the absorbed solute is an ionised molecule or a polar one. In this paper, only the absorption of polar molecules is considered. The electrophoretic flow N_e is modelled as an electric (convective) drift flow directed normally to the surface of the droplets, as:

$$N_e = v_e y \tag{13}$$

Where v_e is the modulus of the electrical drift velocity (Raizer, 1991; Sinha and De, 2012), defined as:

$$v_e = \mu F_e \tag{14}$$

In Eq. (14) μ (m·N^{-1}·s^{-1}) is the solute thermal mobility:

$$\mu = \frac{D_g}{kT} \tag{15}$$

and F_e (N) is the modulus of the electric force acting between the charged water drop surface and the solute.

For the absorption of a polar molecule, F_e can be expressed as:

$$F_e = p\nabla E = -\frac{4pq}{\pi\varepsilon_0 d_{32}^3} \tag{16}$$

where: q (C) is the ion charge, p (C·m) is the electric dipole moment of the molecule; ε_0 (C^2·m^{-2}·N^{-1}) is the vacuum permittivity, ∇E is the gradient of the electric field generated by the droplet close to its own surface. In Eq. (16) the force is calculated close to the droplet interface: the size of the gas film surrounding the droplet is neglected. Finally, it is worth noticing that the sign minus in Eq. (16) indicates that the force is directed toward the droplet regardless of the sign of the droplet charge: while for an ionic solute the electrophoretic terms can be either repulsive or attractive depending on the polarity of the droplets and the charges of the ions, for a dipolar molecule the polarity of the net charge applied over the droplet is meaningless. This result is consistent with former experiments (Di Natale et al., 2020; Matteson et al., 1972; Uchigasaki et al., 1967; Vasishtha and Someshwar, 1988) that showed that the absorption rate of charged sprays is independent on the sign of their charge.

The electrophoretic flux thus becomes:

$$N_e = \frac{4D_g pq}{\pi\varepsilon_0 kTd_{32}^3} y = k_e y \tag{17}$$

Where the term k_e is the electrophoretic coefficient (m·s^{-1}).

In light of the larger mass flux in the gas phase, the interfacial condition (x_I, y_I) deriving from Eq. (12) becomes:

$$y_I = \frac{m(q)(k_g + k_e)y + k_l y^*}{m(q)k_g + k_l} = \alpha y + \beta y^* \tag{18}$$

Being $m(q)$ the partition factor for charged droplets, which will be discussed in detail later in this section, while α and β are:

$$\alpha = \frac{m(q)(k_g + k_e)}{m(q)k_g + k_l} \tag{19}$$

$$\beta = \frac{k_l}{m(q)k_g + k_l} \tag{20}$$

The assessment of the partition factor for charged droplets is the most complex issue of this work. As anticipated, a similar effect has been suggested in the pioneering work of Matteson and Giardina (1974) who correlated the SO_2 absorption rate of charged droplets with an increase in the spreading pressure of SO_2, which is expected as the result of the well-known reduction of surface tension for charged droplets (Di Natale et al., 2019, 2018, 2016; Hohman et al., 2001a, 2001b; Santos et al., 2011). Indeed, despite the large literature regarding the experimental and modelling assessment of gas solubility in different liquids, to the best of our knowledge, the problem of assessing how it changes with the liquid charge has received little attention so far.

The development of a dedicated model for the solubility of charged liquid is well beyond the ambition of this work and, to solve this issue, we propose a simplified approach to correlate interfacial solubility and surface charge density based on the cavity-based approach, "a very clever and insightful idea" (Goldman, 1985), proposed by Sisskind and Kasarnowsky (1933) almost one century ago. According to this approach, the energy involved in the transfer of a molecule from the gas to the liquid phase can be decomposed in two terms, a first one related to the creation of a cavity in the dense liquid interface and a second one related to the specific chemical interactions among the solute and the liquid molecules. Following this approach, Uhlig (1937) proposed a semiempirical model for gas solubility in very dilute solutions. Based on several experiments and a simplified analysis of the interfacial thermodynamics, Uhlig (1937) stated that if we consider a spherical gas molecule to enter the liquid, the energy required to generate the spherical cavity in the liquid interface is associated with the energy required to overcome the surface tension σ_0 (N·m) plus an additional energy term to account for the interaction of solvent and solute molecules, E_a, (kg·m^2·s^{-2}). Under this approach, Uhlig correlated the microscopic problem to a macroscopic, measurable, parameter, such as the surface tension. According to Uhlig model (1937), the partition factor m_0 is:

$$ln(m_0) = \frac{4\pi r_m^2 \sigma_0 - E_a}{kT} \tag{21}$$

Where k (J·K^{-1}) is the Boltzmann constant and r_m (m) is the solute molecular radius. Uhlig model has been successfully applied to describe the solubility of several gas species in liquids having different surface tensions. However, it remained an empiric model whose validity is restricted to low solute concentrations and to those conditions when the interaction energy E_a is reasonably constant regardless of the concentration of the solute. Despite these limitations, this approach appeared promising for our application. In fact, as discussed elsewhere (Di Natale et al., 2019, 2018, 2016; Hohman et al., 2001a, 2001b; Santos et al., 2011), the presence of an electric charge at the interface of a liquid sheet or droplet gives rise to an electric force that counterbalances the surface tension of the liquid (Dreyer et al., 2018; Tinsley et al., 2006). The classical Lippmann (Dreyer et al., 2018; Láng, 2020; Lippmann, 1875; Marichev, 2010) equation correlates surface tension and surface charge. In the case of charged droplets the Lippmann equation can be expressed as:

$$\sigma = \sigma_0 \left[1 - \left(\frac{q}{q_R}\right)^2\right] \tag{22}$$

where q and q_R, in (C), indicate the droplet charge at a given potential and in correspondence with the Rayleigh limit respectively (Rayleigh, 1882; Thaokar and Deshmukh, 2010). It is worth noticing that also the reduction of surface tension is independent of the sign of the applied charge.

If sustained by enough information to define the parameters occurring in the Eqs. (21)–(22), *i.e.* σ_0, r_m, E_a and q/q_R, the Uhlig model can be used to establish a dependence between the droplet's charge density and the interfacial solubility. Accordingly, the interfacial solubility of a given solute in the case of charged droplets, $m(q)$ is:

$$\ln m(q) = \frac{4\pi r_m^2 \sigma_0 \left[1 - \left(\frac{q}{q_R}\right)^2\right] - E_a}{kT} \tag{23}$$

In light of the larger mass transfer rate in the gas film deriving from the electrophoretic contribution, the definition of an overall mass transfer coefficient is less straightforward, and it is more convenient to refer to the mass transfer rate to the gas film transport.

Accordingly, the model describing the absorption of a dipolar solute into a charged droplet exposed to a gas phase at solute concentration y (Eqs. (10)–(11)) can be written in an implicit form as:

$$\frac{dn}{dt} = k_g A \left[(1-\alpha)y - m(q)\beta \frac{n}{V_d}\right] + k_e A y \tag{24}$$

The same initial condition of Eq. (10) holds.

A scheme of the main features of the mass transfer model for uncharged and charged droplets is shown in Fig. 1.

3. Results and discussion

3.1. Model validation

To allow a proper application of Eq. (24), it is necessary to address the size distribution, the morphology, the velocity and the charge of sprayed droplets. In the largest majority of the existing dataset provided by former papers, sprays are used (Di Natale et al., 2019). This implies that the absorption involves an ensemble of droplets with different sizes, trajectories and charges. Besides, in these works, much of the information required to sustain the application of Eqs. (12)–(24) was not provided. This makes complex and often unreliable the validation of the proposed model. A few studies, such as the one of Matteson and Giardina (1974) and Di Natale et al. (2020), make use of trains of droplets to investigate the absorption of SO_2 by charged sprays. With respect to other studies available in the literature (Di Natale et al., 2022, 2019; Li et al., 2022), these experimental results have other advantages: firstly, the use of electrospray in dripping and microdripping mode avoids the formation of jets and generates trains of uniform droplets emitted at an almost constant frequency. Second, it reduces the fluid dynamic complexities related to the analysis of a continuous counter-current spray tower. Unfortunately, Matteson and Giardina (1974) did not provide information on droplets' charge and although there are some correlations to the average size and charge density of electrosprayed droplets (Agostinho et al., 2018; Eggers and Villermaux, 2008; Ganán-Calvo, 2004; Manna et al., 2017; Rosell-Llompart et al., 2018), these are not validated for the experimental conditions of interest. Besides, the work of Matteson and Giardina (1974) does not include information on droplet morphology.

To overcome these limitations, following the Matteson and Giardina approach and on the bases of former experience on particle removal by charged droplets (D'Addio et al., 2014, 2013), our group has developed an experimental methodology aimed to provide sufficient information to sustain the absorption modelling (Di Natale et al., 2020). This methodology makes use of a closed vessel filled with gas at a fixed initial concentration of the desired trace solute put into contact with a train of almost identical water droplets injected into the chamber through an electrospray assembly, operated in the dripping mode under different electrical potentials. During the experiments, the concentration of the solute in the gas phases was reduced as a consequence of the adsorption on the set-up walls and losses in the sampling lines (these phenomena are referred to as baseline depletion in the original work and thereinafter) and of the absorption of the solute into the liquid phase. Experiments have been suitably performed to decouple baseline depletion and gas absorption. The outcomes of this experimental methodology are records of solute concentration in the gas volume as a function of the time of exposure to the absorbing liquid spray. The methodology also includes dedicated optical and electrical analyses to estimate droplets' size, morphology and charge, as well as their time of formation and their falling time in the vessel.

The method has been applied to describe the absorption of SO_2 from an air stream into charged drops of distilled water acidified with HCl so to assure that the interfacial solubility can be well expressed by the constant partition factor (*i.e.* the Henry law) equation. This system has been chosen both for its relevance in atmospheric phenomena and chemical engineering processes (Di Natale et al., 2022, 2020; Flagiello et al., 2019; Giberti and Hassanali, 2017; Gong and Li, 2021; Jiang et al., 2020; Pruppacher and Klett, 2010; Seinfeld and Pandis, 1998; Sharif et al., 2021; Valluri and Kawatra, 2021; Zhou and Wang, 2020).

Experimental results are resumed in Fig. 2 in terms of the time course

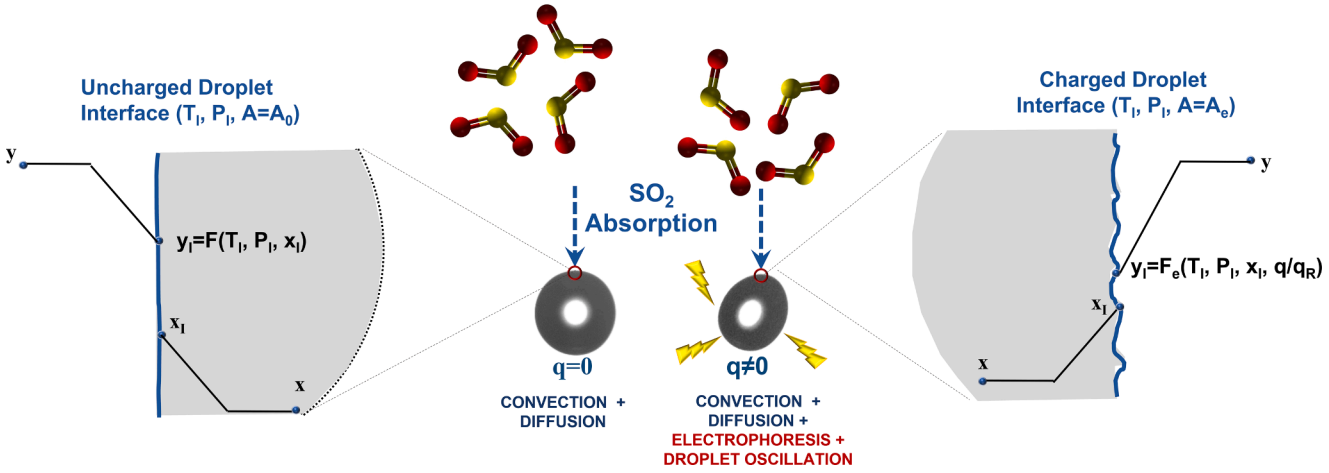

Fig. 1. Main features of the mass transfer model for uncharged (left) and charged (right) droplets.

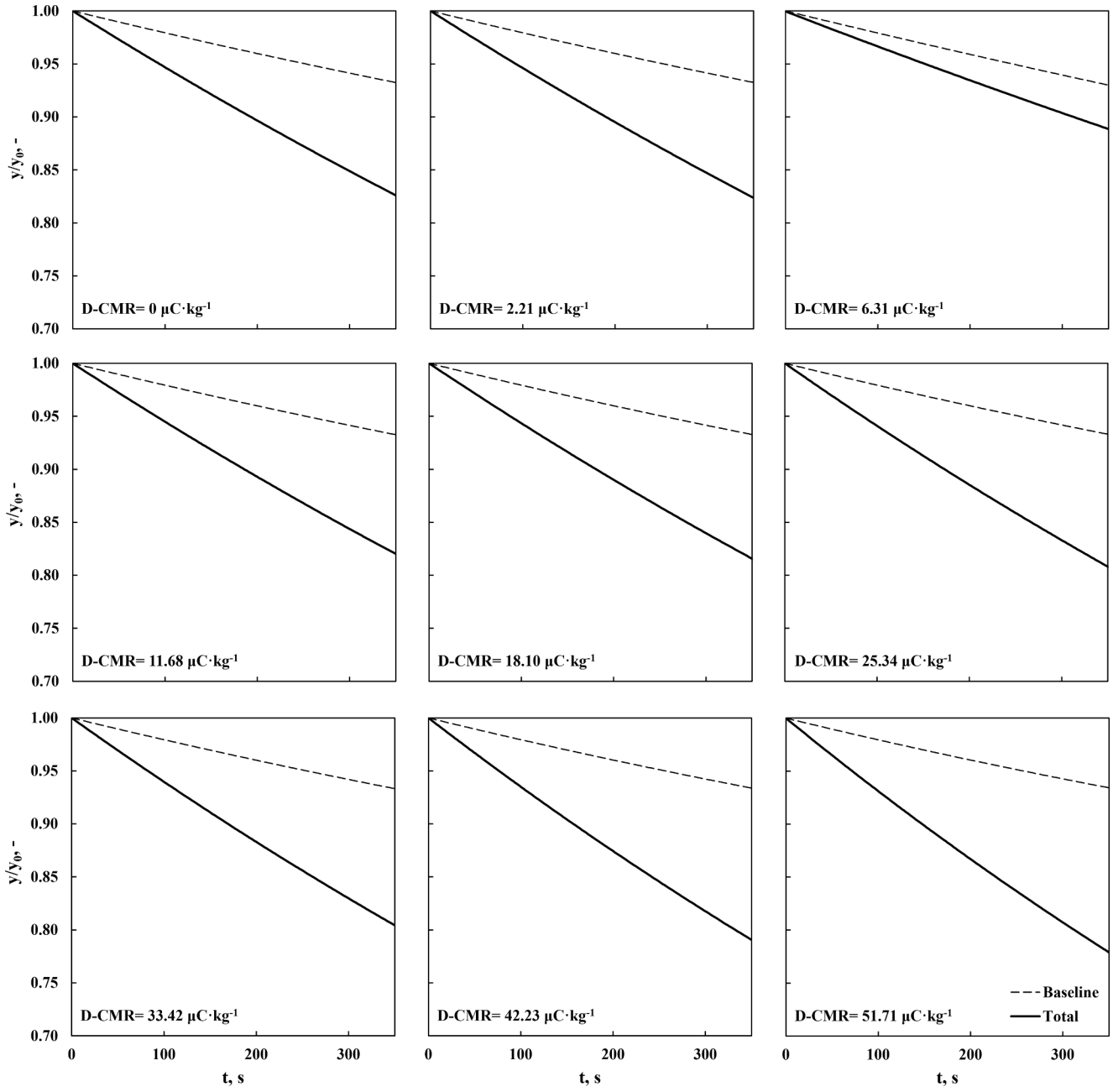

Fig. 2. Time course of SO_2 concentration in the closed vessel as a function of the D-CMR for negatively charged droplets. Similar results hold for positively charged droplets.

of SO_2 concentration in the closed vessel as a function of the droplets charge to mass ratio, D-CMR, ($\mu C \cdot kg^{-1}$), which is the ratio between the absolute value of droplet charge and mass. Indications of the droplets' spray frequency f (Hz), average Sauter diameter, d_{32} (m), mean droplet area, A (m^2) deformation, D (-), the ratio between the maximum to minimum drop surface area $1 + \varepsilon$ (-), droplet formation time, τ_p (s) and droplet falling time, τ_f (s) can be retrieved from experiments and are reported in Table 1 as a function of D-CMR, ($\mu C \cdot kg^{-1}$).

The SO_2 depletion related to the vessel wall is also measured and is indicated as Baseline in Fig. 2. The experiments revealed that the baseline was not altered if the electric potential was applied to the electrospray assembly but water was not fed into the vessel.

It is also worth noticing that the SO_2 absorption rate is not altered by the droplets' charge polarity (Di Natale et al., 2020). Therefore, for the sake of simplicity, Table 2 and Fig. 2 only refer to the case of negatively

Table 1
Parameters adopted in the calculations as a function of the density of electric charges deposited over the droplets (D-CMR, $\mu C \cdot kg^{-1}$).

D-CMR, $\mu C \cdot kg^{-1}$	d_{32}, mm	*D*, -	$1 + \varepsilon$, -	*A*, mm^2	*f*, s^{-1}	τ_p, s	τ_f, s
0	2.57	0.013	1.129	17.01	1.87	0.533	0.062
2.21	2.23	0.014	1.127	11.75	2.70	0.369	0.062
6.31	2.26	0.013	1.136	11.63	2.74	0.365	0.062
11.58	2.23	0.044	1.382	10.73	2.97	0.335	0.062
18.10	2.20	0.030	1.119	10.75	2.96	0.337	0.062
25.34	216	0.040	1.111	10.14	3.14	0.318	0.062
33.52	2.10	0.037	1.143	9.36	3.48	0.294	0.062
42.23	2.04	0.031	1.135	8.43	3.78	0.264	0.062
51.71	1.93	0.040	1.159	7.11	4.48	0.222	0.062

Table 2
Summary of mass transfer coefficient models k_g and k_l [m·s] for oscillating droplets (Flagiello et al., 2019).

Handlos and Baron (1957)	$k_l = \omega\sqrt{\frac{D_l U}{d_{32}}\cdot\left(\frac{\rho_g C_D}{2\rho_l}\right)}$ $k_g = \frac{\left(2+0.6Re_g^{0.5}Sc_g^{0.5}\right)\cdot D_g}{d_{32}}$
Rose and Kintner (1966)	$k_l = 0.450\cdot(D_l\omega)$ $k_g = \frac{\left(2+0.6Re_g^{0.5}Sc_g^{0.333}\right)\cdot D_g}{d_{32}}$
Brunson and Wellek (1970)	$k_l = 2\cdot\sqrt{\frac{d_{32}\omega}{\pi}}\cdot(1+0.687\varepsilon)\cdot\left(\frac{D_l}{d_{32}}\right)$ $k_g = \left[\frac{4}{\pi}\sqrt{\frac{d_{32}^2\omega}{4D_g}\cdot\left(1+\varepsilon+\frac{3}{8}\varepsilon^2\right)}\right]\cdot\left(\frac{D_g}{d_{32}}\right)$
Yamaguchi et al. (1975)	$k_l = 1.14\cdot\left(\frac{d_{32}^2\omega\rho_l}{\mu_l}\right)^{0.56}\cdot\left(\frac{D_l}{d_{32}}\right)$ $k_g = 1.4\cdot\left(\frac{d_{32}^2\omega\rho_g}{\mu_g}\right)^{0.5}\cdot Sc_g^{0.5}\cdot\left(\frac{D_g}{d_{32}}\right)$
Clift et al. (1978)	$k_l = 2\cdot\sqrt{\frac{D_l\omega}{\pi}}\cdot\sqrt{1+\varepsilon+\frac{3}{8}\varepsilon^2}$ $k_g = \frac{1.2}{\sqrt{D_g}}\cdot\left[\frac{48d_{32}\sigma}{\pi^2(2\rho_g+3\rho_l)}\right]^{0.25}\cdot\left(\frac{D_g}{d_{32}}\right)$

charged droplets.

Each experimental run consists of the measure of the time course of SO_2 concentration with the water switched off (baseline depletion) and with the charged spray in operation. The baseline depletion has been modelled as:

$$V\frac{dy}{dt} = -r_w = -\Lambda_w^0 y \tag{25}$$

With initial conditions:

$$t = 0;\ y = y_0 \tag{26}$$

where y (mol·m^{-3}) and y_0 (mol·m^{-3}) are, respectively, the instantaneous and the initial SO_2 gas concentrations in the vessel having volume V. The term r_w (mol·s^{-1}) indicates the baseline depletion of SO_2, which can be well described by a first-order rate model (Di Natale et al., 2020), and Λ_w° is the baseline scavenging parameter. As described in Di Natale et al. (2020) Λ_w° has been measured from the best-fitting of every single experiment, by using Eq. (25). Although on average Λ_w° has been estimated as $4.7{\cdot}10^{-7}$ m^3 s^{-1} ± 12%, we used the specific experimental value to describe each test run.

The time course of gas SO_2 concentration when the charged spray is switched-on has been modelled as the sum of the baseline depletion and the absorption into the sprayed droplets, r_s (mol·s^{-1}), neglecting second-order effects. Accordingly, the mass balance on SO_2 into the gas volume inside the vessel is:

$$V\frac{dy}{dt} = -r_w - r_s \tag{27}$$

As a general rule, the r_s term should consider the amount of SO_2 absorbed by each of the, say, K droplets present in the vessel at time t. Therefore, r_s should be expressed as the sum of the absorption rate of each k^{th} droplet as:

$$r_s = \sum_{k=1}^{K}\frac{dn_k}{dt} \tag{28}$$

This expression includes the contribution of droplets during different moments of their lifetimes: at any given time, t, there is one droplet forming at the nozzle tips, while others are travelling along the vessel.

For the numerical integration of Eq. (27), we can use an explicit discretization scheme, under which we assume that all physical and chemical properties of the system in the time interval $\Delta t_i = t_{i+1}$-t_i are assumed equal to those at time t_i. Under this scheme, Eqs. (27)–(28) can be approximated to calculate the concentration in the vessel at time t_{i+1}, y_{i+1}, as:

$$y_{i+1} = y_i - \frac{\Delta t_i}{V}\left[\Lambda_w^0 y_i + r_{s,i}\right] \tag{29}$$

$$t_i = 0;\ \ y_i = y_0; \tag{30}$$

Where $r_{s,i}$ is the average spray absorption rate calculated for a constant gas concentration of y_i and for the time interval $\Delta t_i = t_{i+1}$-t_i.

The characteristics of the experimental system allow simplifying the expression of $r_{s,i}$ thanks to some considerations. First, it is worth noticing that electrosprays exerted in dripping or microdripping modes, as those adopted here, are characterised by the generation of a train of almost identical droplets, with similar size, charge and trajectories. Then, it must be noticed that during the experiments, the droplets spent at most 0.533 s as a pendant drop forming at the nozzle tip and at most 0.062 s as a droplet falling from the nozzle tip to the vessel walls (Table 2). Their dynamic is therefore hundreds of times faster than the observed evolution of SO_2 concentration in the vessel: during the lifetime of a droplet, the concentration of SO_2 in the gas phase can be assumed constant and uniform in the vessel volume. It is also worth mentioning that the droplets' lifetime is also smaller than the sampling time of the gas analyser used in the experiments. In light of these considerations, it is possible to estimate an average contribution of droplets to the absorption rate in a time interval $\Delta t_i = t_{i+1}$-t_i as:

$$r_{s,i} = \frac{1}{\Delta t_i}\int_{t_i}^{t_{i+1}}\left[\sum_{k=1}^{K}\frac{dn_k}{dt}\right]dt = f\cdot n_{D,i} \tag{31}$$

Where f (Hz) is the frequency of droplets emitted per unit of time by the needle, which can be retrieved from the experiments, and $n_{D,i}$ is the

amount of SO_2 absorbed by a generic droplet during its entire lifetime (from the instant the former droplet leaves the needle to the instant in which the droplet hits against the bottom wall of the vessel), when it is exposed to a gas containing a concentration y_i of SO_2 during the time interval Δt_i.

In this experimental setup, the amount of SO_2 absorbed in each droplet, n_{Di}, is composed of two parts. The first one, named $n_{p,i}(\tau_p)$ corresponds to the amount of SO_2 absorbed by the pendant droplet forming at the needle tip from its first appearance to the time of its detachment, τ_p (s). A second part, named $n_{f,i}(\tau_f)$ accounts for the amount of SO_2 acquired by the falling droplet from its detachment from the needle tip, τ_p, until its collision with the vessel wall after τ_f seconds – its lifetime. The separation of the two contributions is important here, both because of the physical differences between a pendant and a falling droplet and because of the comparable time spent by a droplet in each of the stages. As anticipated, the selection of dripping mode for the electrospray operation allows for a further simplification of the absorption process since it avoids jetting conditions and allows for approximating the droplet formation step as the growth of a spherical interface.

According to these considerations, the rate of SO_2 absorbed by each droplet during its lifetime is:

$$n_{D,i} = n_{p,i}(\tau_p) + n_{f,i}(\tau_f) \tag{32}$$

The value of $n_{p,i}(\tau_p)$ is calculated from the integration of the Eq. (24) between $\tau = 0$ and $\tau = \tau_p$, which refers to the case of droplet formation:

$$\frac{dn_{p,i}}{d\tau} = k_{g,p}(\tau)A(\tau)\left[(1-\alpha(\tau))y_i - m(q)\beta(\tau)\frac{n_{p,i}}{V_d(\tau)}\right] + k_e(\tau)A(\tau)y_i \tag{33}$$

The time τ denotes the age of the droplet from its first appearance at the needle tip ($\tau = 0$). Since an SO_2-free liquid is pumped into the vessel, the initial condition is:

$$\tau = 0; \quad n_{p,i} = 0 \tag{34}$$

The value of $n_{f,i}(\tau_f)$ is calculated from the integration of the Eq. (24) between $\tau = \tau_p$ and $\tau = \tau_f$, aimed to describe droplet fall:

$$\frac{dn_{f,i}}{dt} = k_{g,f}A\left[(1-\alpha)y_i - m(q)\beta\frac{n_{f,i} + n_{p,i}(\tau_p)}{V_d}\right] + k_e A y_i \tag{35}$$

The initial condition for this integration now refers to the case of the droplet leaving the nozzle tip at time τ_p, when the droplet contains $n_{p,i}(\tau_p)$ moles of SO_2, but the amount absorbed during the droplet fall $n_{f,i}$ is still null:

$$\tau = \tau_p; \quad n_{f,i} = 0 \tag{36}$$

In Eqs. (33) and (35) $k_{g,p}(\tau)$ and $k_{g,f}$ in ($m \bullet s^{-1}$) are the gas film mass transfer coefficients during droplet formation and fall; $A(\tau)$ (m^2) and $V_d(\tau)$ (m^3) are the droplet surface area and volume during its formation; A (m^2) and V_d (m^3) are the droplet surface area and volume during fall.

It is worth noticing that in Eq. (33) the gas film mass transfer coefficient $k_{g,p}(\tau)$, the droplet surface area $A(\tau)$ and, of course, the droplet volume $V(\tau)$ are considered as time variables since droplets change their size during formation. Similarly, during droplet formation, the droplet diameter and the liquid film mass transfer coefficient are a function of the droplet lifetime, $d_{32}(\tau)$ and $k_{l,p}(\tau)$. Accordingly, the terms α, β and k_e are a function of the droplet lifetime in this equation. Differently, the same variables can be assumed constant in Eq. (35).

Furthermore, it must be also noticed that it was assumed that the value of $m(q)$ for a pendant drop is equal to the value of the subsequent falling drop, assuming that the charge density of the jet is the same as the sprayed droplets, as commonly reported in electrohydrodynamic atomization studies (Cloupeau and Prunet-Foch, 1989; Jaworek and Krupa, 1999; Wei et al., 2018).

The SO_2 equilibrium absorption by uncharged water has been measured according to the procedure adopted by Flagiello et al. (2018), and has a value of $m_0 = 36.55$ which is consistent with the literature findings (Seinfeld and Pandis, 1998).

Approximating the solute molecular radius r_m as the length of the double bond S=O, which is equal to 1.2391 Å (Matito-Martos et al., 2014), Eq. (21) can be used to estimate the chemical interaction term E_a, which resulted equal to $-7.22 \cdot 10^{-22}$ ($kg \cdot m^2 \cdot s^{-2}$). This value indicates that the contribution to SO_2 solubility of the chemical interaction term is around 5% of the surface tension contribution. Assuming that the interaction energy of the solute is independent on the droplet charge density. After the determination of E_a, the interfacial solubility for charged droplets can be estimated from Eq. (23).

As regards the effect of droplet morphologies, it must be recalled that the actual size and shape of the droplets have been obtained from the image analyses and are partially resumed in Table 1. The experiments revealed that the falling droplets are deformed and oscillating, while the pendant drops are mostly spherical, especially for large D-CMR.

To estimate the mass transfer coefficient for the formation of the droplets, we used the model of Angelo et al. (1966), which considered the forming droplet as a growing sphere:

$$k_{g,p}(\tau) = \frac{\left[2 + 0.6Re_g^{0.5}(\tau)Sc_g^{0.5}\right]D_g}{d(\tau)} \tag{37}$$

$$k_{l,p}(\tau) = \sqrt{\frac{4D_l}{\pi\tau_p}} \tag{38}$$

For this model, the diameter of the forming droplet $d(\tau)$ (m), and the gas Reynolds number during formation $Re_g(\tau)$ are given by the following expressions:

$$d(\tau) = \left(\frac{6Q\tau}{\pi}\right)^{1/3} \tag{39}$$

$$Re_g(\tau) = \frac{\rho_g u d(\tau)}{\mu_g} \tag{40}$$

Where Q ($L \cdot s^{-1}$) is the water flow rate. The volume of the forming droplet is given by the product between the liquid flow rate Q and the formation time τ, while the surface area $A(\tau)$ is that of a sphere having a diameter $d(\tau)$.

In light of the availability of several models to describe the mass transfer coefficients for a falling droplet, we prefer to compare their capacity to predict the experimental data instead of arbitrarily selecting one of them. Three categories of mass transfer models for droplets have been considered:

- Non-oscillating droplets – stagnant flow models
- Non-oscillating droplets – internal circulation flow models
- Oscillating droplets models

It is worth remembering that the optical analysis reveals that droplets are deformed and subjected to oscillatory motions, which leads to conceptually preferring the last category of models.

Table 2 resumes the formulation of several mass transfer models for k_g and k_l ($m \cdot s^{-1}$) valid for droplets of a Newtonian liquid under oscillating internal flow and unsteady oscillating external flow conditions (Flagiello et al., 2019), which are likely to be found in the case of falling water droplets having a size larger than 1700 μm (Clift et al., 1978; Klee and Treybal, 1956; Lamb, 1975; Yeh, 2002).

When necessary, mass transfer coefficients are calculated using the actual surface tension as a function of the droplet charge, as in Eq. (22).

Being y_i constant, Eqs. (33) and (35) are first-order linear ODEs of the generic form:

$$\frac{dn_i}{d\tau} = \gamma(\tau) - \delta(\tau)n_i \tag{41}$$

With initial condition:

Table 3
Determination factor R^2 between experimental results and model predictions for the different mass transfer models.

D-CMR, μC·kg^{-1}	Clift et al. (1978)	Handlos and Baron (1957)	Rose and Kintner (1966)	Brunson and Wellek (1970)	Yamaguchi et al. (1975)
0	0.995	0.926	0.961	0.997	0.997
2.21	0.992	0.794	0.874	0.967	0.990
6.31	0.965	0.789	0.798	0.919	0.957
11.58	0.996	0.786	0.876	0.983	0.993
18.10	0.986	0.993	0.839	0.953	0.982
25.34	0.979	0.689	0.809	0.936	0.972
33.42	0.996	0.741	0.867	0.898	0.994
42.23	0.998	0.739	0.864	0.974	0.995
51.71	0.989	0.802	0.926	0.977	0.996
Mean	0.990	0.810	0.870	0.960	0.990
Variance	1.0·10^{-4}	1.0·10^{-2}	2.5·10^{-3}	9.0·10^{-4}	1.0·10^{-4}

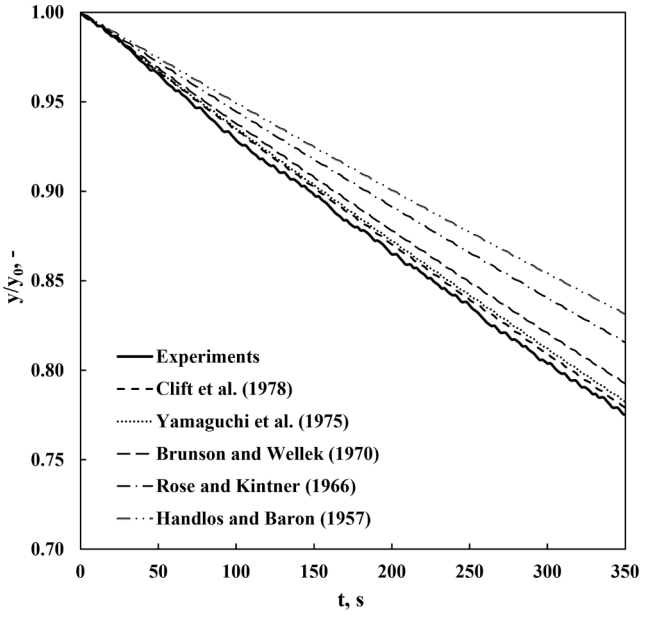

Fig. 3. Time course of the dimensionless SO_2 molar fraction y/y_0 for a D-CMR = 42.23 μC·kg^{-1}: comparison between experiments and model prediction for the different oscillating mass transfer models.

$$\tau = \tau_0 \quad n_i = n_{i0} \tag{42}$$

For Eq. (33) the coefficients $\gamma(\tau)$ and $\delta(\tau)$ are a function of the droplet lifetime τ_f, while for Eq. (35), they are constant.

The analytical solutions of such equations is (Matsuda, 1980):

$$n_i(\tau) = exp\left[-\int_{\tau_0}^{\tau_f}\gamma(\tau)d\tau\right]\cdot\left[n_{i0}+\int_{\tau_0}^{\tau_f}\delta(\tau)\cdot exp\left(\int_{\tau_0}^{\tau_f}\gamma(s)ds\right)d\tau\right] \tag{43}$$

The integral of the functions $\gamma(\tau)$ and $\delta(\tau)$ can be calculated with conventional numerical methods. In our case, we used the trapezoidal rule with a $\Delta\tau = 0.001$ s.

To sum up, starting from the initial condition of Eq. (30), for each time t_i at which the concentration is y_i, the algorithm calculates $n_{D,i}$ from solutions of Eqs. (32)–(36), then the value of $r_{s,i}$ (Eq. (31)) and calculate y_{i+1} from Eq. (29). Then, another iteration starts.

The experimental data are compared with model predictions in terms of the Determination Factor R^2 defined as:

$$R^2 = 1 - \frac{RSS}{TSS} \tag{44}$$

Where *RSS* and *TSS* are the residual sums of squares and the total sum of squares, given by the following equations:

$$RSS = \sum_{i=1}^{J}\left(y_{i,exp} - y_{i,mod}\right)^2 \tag{45}$$

$$TSS = \sum_{i=1}^{J}\left(y_{i,exp} - y_{avg}\right)^2 \tag{46}$$

Where $y_{i,\mathrm{exp}}$ and $y_{i,mod}$ are the experimental and modelling values of the gas concentrations at a generic time t_i and y_{avg} is the mean value of the experimental data. To simplify the calculation of RSS and TSS, we "synchronised" the model and the experimental time, by using a discretization time, Δt_i equal to the sampling time of the experiments, *i.e.* 1 s. In this way, the time t_i of the experiments coincided with the time t_i of the model and $y_{i,\mathrm{exp}}$ and $y_{i\ mod}$ are virtually simultaneous.

In the following, we compared the model prediction and the experiment by considering separately:

Table 4
Determination factor R^2 between experimental results and model predictions obtained for non-oscillating droplets – internal circulation flow models (Flagiello et al., 2019).

D-CMR, μC·kg^{-1}	Lochiel and Calderbank (1964)	Garner and Tayeban (1960)	Griffith (1960)	Hughmark (1967)	Saboni and Alexandrova (2001)
0	0.733	0.734	0.734	0.734	0.735
2.21	0.745	0.744	0.744	0.744	0.743
6.31	0.815	0.816	0.816	0.816	0.817
11.58	0.752	0.752	0.847	0.752	0.750
18.10	0.827	0.827	0.827	0.826	0.824
25.34	0.806	0.805	0.805	0.805	0.801
33.42	0.766	0.796	0.810	0.804	0.804
42.23	0.881	0.879	0.880	0.879	0.882
51.71	0.813	0.811	0.812	0.811	0.807
Mean	0.790	0.800	0.810	0.880	0.800
Variance	2.5·10^{-3}	2.5·10^{-3}	2.5·10^{-3}	2.5·10^{-3}	2.5·10^{-3}

Table 5
Determination factor R^2 between experimental results and model predictions obtained for non-oscillating droplets – stagnant flow models (Flagiello et al., 2019).

D-CMR, μC·kg^{-1}	Davies (1972)	Danckwerts (1970)	Dou et al. (2009)
0	0.684	0.543	0.585
2.21	0.696	0.542	0.587
6.31	0.766	0.612	0.657
11.58	0.778	0.546	0.591
18.10	0.757	0.621	0.667
25.34	0.717	0.599	0.645
33.42	0.832	0.557	0.603
42.23	0.879	0.670	0.716
51.71	0.764	0.596	0.644
Mean	0.745	0.587	0.633
Variance	1.8·10^{-3}	1.6·10^{-3}	1.6·10^{-3}

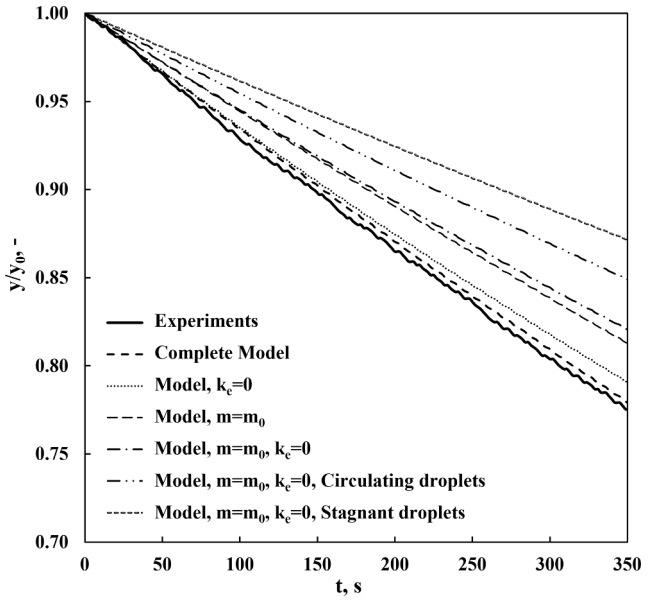

Fig. 4. Comparison between experimental data (D-CMR = 42.23 μC·kg^{-1}) and model prediction with the complete formulation (including the observed droplets oscillation) and applied neglecting specific terms (*e.g.* placing k_e = 0 and/or m = m_0) or considering different droplets mass transfer conditions.

- The morphological effects related to the occurrence of deformed and oscillating droplets, which were included by comparing different mass transfer models;
- The influence of droplet charge on the interfacial solubility;
- The relevance of the electrophoretic contribution.

As a first result, we compare in Table 3 the determination factor R^2 for different predictive mass transfer models valid for oscillating droplets models, which are expected to better describe our dataset.

Table 3 shows that almost all the models provide a very good prediction of experimental data with better results for the equations of Clift et al. (1978) and Yamaguchi et al. (1975), which provided R^2 always above 0.96. The model of Handlos and Baron (1957) provided the worst prediction, although the values of R^2 are above 0.70. This result can be explained by considering that this model is the extrapolation of a model born to describe circulating flows (Brunson and Wellek, 1970; Clift et al., 1978).

Fig. 3 shows a comparison between the experimental and modelled time course of the dimensionless SO_2 molar fraction y/y_0 at D-CMR = 42.23 μC·kg^{-1} for the different mass transfer models. The plots clearly show the discrepancies between the experimental and model prediction and further testify how the Clift et al. (1978) and Yamaguchi et al. (1975) models provided the optimal prediction of the absorption over the duration of the entire experiment.

The model predictions using equations for non-oscillating droplets in the case of internal circulation and stagnant flows, neglecting the droplets deformation generated by electrospray are shown in Tables 4 and 5. The results revealed that the model prediction worsens by an average of around 12% for internal circulation flow and 33% for stagnant flows.

To investigate the contribution provided by the different terms associated with the droplets' charge density to the absorption process (*i.e.* the interfacial solubility, the deformation and the electrophoresis), the same model has been applied by removing, one by one, the corresponding equations and models for charged droplets. As an example, Fig. 4 shows a comparison between different model formulations for the case of D-CMR = 42.23 μC·kg^{-1} using the Clift et al. (1978) model for mass transfer coefficients. Similarly, Tables 6 show the values of the determination factor R^2 achieved by comparing the experimental data with: i) the model predictions in absence of electrophoretic contribution; ii) the model predictions obtained for $m(q) = m_0$ with electrophoretic contribution; iii) the model predictions for for $m(q) = m_0$ in absence of electrophoretic contribution. The Clift model is used to describe the mass transfer coefficient during the droplet fall, but the same conclusions hold for all the other models reported in Table 2.

As shown, there is a small effect of electrophoresis, which contributed to almost 1% of the model prediction, while using the interfacial solubility values for uncharged droplets (*i.e.* the partition factor m_0 in place of $m(q)$) worsens the model prediction by about 7%, on average, with over 13–14 percentage points for larger droplet charge level. The effect associated with electrophoresis is also evident when considering the presence of this contribution using the same partition factor m_0 that holds for uncharged droplets: a little improvement in the model prediction, less than about 4% is observed by including k_e in the model calculation.

These results indicate that while the electrophoretic contribution to mass transfer rate plays a limited role in the absorption rate in these experimental conditions, the assessment of droplet charge density effects on the interfacial solubility and the deformation of droplets is required to assure an appropriate description of the experiments.

In conclusion, once a correct assessment of fluid dynamic conditions and droplet charge levels is available, the model predicts in a very accurate way the experimental data.

3.2. Model application – Effect of process parameters

The mass transfer model of Eq. (24) is virtually applied to describe some reference conditions with the aim of exploiting the effects of droplet size and charge on the absorption rate. In particular, the

Table 6
Determination factor R^2 between experimental results and model predictions neglecting specific contributions to electrophoretic flow and interfacial solubilities. The Clift model is used to describe the mass transfer coefficient during droplet fall.

D-CMR, μC·kg^{-1}	$k_e = 0$	$m(q) = m_0$	$k_e = 0$ $m(q) = m_0$	Complete model
0	0.995	0.995	0.995	0.995
2.21	0.984	0.991	0.978	0.992
6.31	0.981	0.961	0.893	0.965
11.58	0.984	0.991	0.976	0.996
18.10	0.970	0.965	0.942	0.986
25.34	0.954	0.922	0.872	0.979
33.42	0.977	0.929	0.846	0.996
42.23	0.984	0.879	0.836	0.998
51.71	0.985	0.885	0.850	0.989
Mean	0.980	0.946	0.910	0.990
Variance	$1.0{\cdot}10^{-4}$	$2.0{\cdot}10^{-3}$	$3.6{\cdot}10^{-3}$	$1.0{\cdot}10^{-4}$

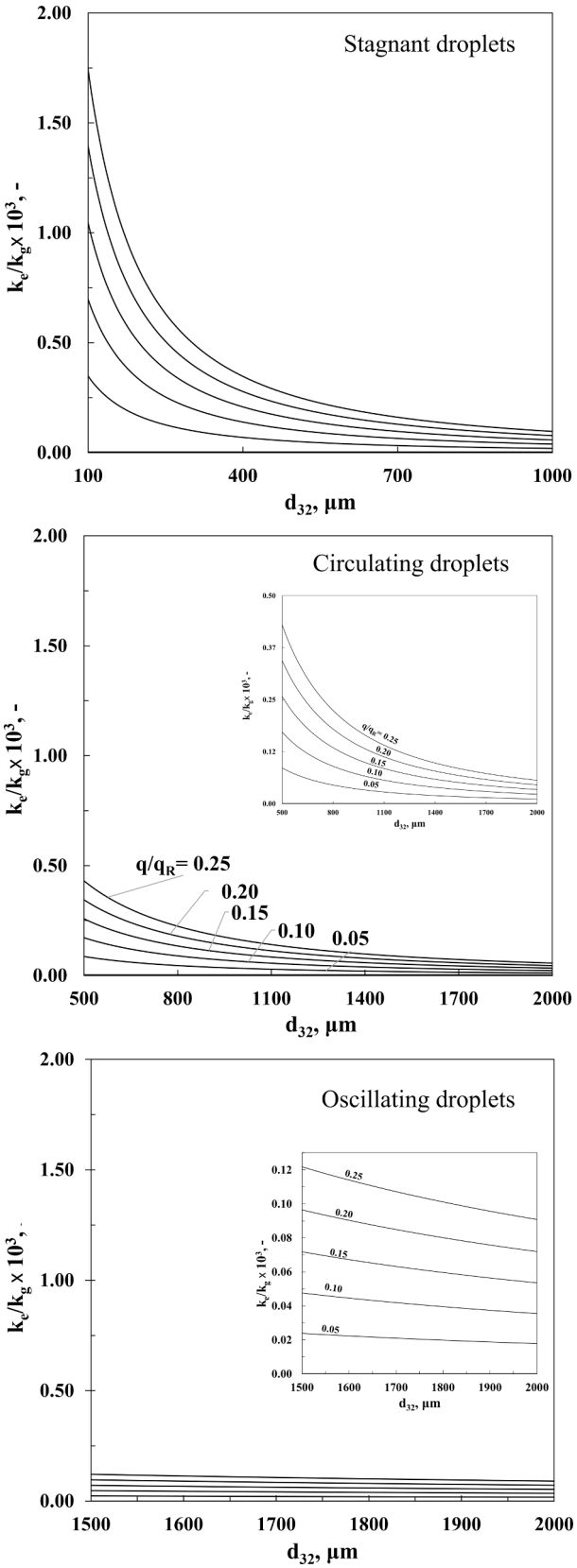

Fig. 5. Ratio between the electrophoretic coefficient k_e and the convective mass transfer coefficient in the gas film k_g as a function of the droplet Sauter diameter (d_{32}) varying the droplet to Rayleigh limit ratio (q/q_R) for stagnant, circulating and oscillating droplets.

following reference conditions have been considered:

a. Spherical droplets having mean Sauter diameters from 100 to 2000 μm falling at their terminal velocity.
b. Droplets charge up to 25% of the Rayleigh limit.
c. Absorption of diluted SO_2 (y_0 = 1000 ppmv in the air at 1 atm and 25 °C) in distilled water droplets containing a concentration of dissolved SO_2 corresponding to two values of y^*: y^*=0; y^*=90 %y_0. These conditions have been chosen to neglect the influence of the global driving force, y-y^*, on the absorption rate. The corresponding value of y_I varied according to Eq. (18).
d. Absorption of diluted SO_2 (y_0 = 1000 ppmv in the air at 1 atm and 25 °C) in distilled water droplets assuming a value of x_0 in the droplet equal to $4.14 \cdot 10^{-4}$ mol/m^3, corresponding to 50% of the equilibrium value at y_0 for uncharged droplets, i.e. $x_0 = 0.5\, y_0/m_0$. This condition has been chosen to fully exploit the effects of droplet charge on the absorption rate, including both the effects on the mass transfer coefficient and the overall driving force, being $y^* = m(q)x_0$. The corresponding value of y_I varied according to Eq. (18).

The model application requires the selection of mass transfer models to represent the different hydrodynamic conditions. According to former studies (Clift et al., 1978; Klee and Treybal, 1956), water droplets finer than 1700 μm are rigid spheres, becoming deformed and oscillating ellipsoids for larger diameters. Wegener et al.(2014) indicated that the mass transfer rate of droplets finer than 500 μm is well described by stagnant models (*e.g.* Danckwerts and Lannus, 1970; Davies, 1972; Dou et al., 2009), while for droplets larger than 1700 μm oscillating models are more representative of the hydrodynamic conditions (*e.g.* Brunson and Wellek, 1970; Clift et al., 1978; Handlos and Baron, 1957; Rose and Kintner, 1966; Yamaguchi et al., 1975). For intermediate sizes, circulating models (*e.g.* Garner and Tayeban, 1960; Griffith, 1960; Hughmark, 1967; Lochiel and Calderbank, 1964; Saboni and Alexandrova, 2001) are preferred. Unavoidably, there are differences in the absolute values of mass transfer coefficients among different models of the same classes, due to their semiempirical origin. To account for such differences, the model has been applied considering the arithmetic average value of the mass transfer coefficients calculated for each class.

We reported here three different sets of charts. The first one (Fig. 5) reports the ratio k_e/k_g, comparing the electrophoretic and the gas convective contribution to the mass transfer in the gas phase, *i.e.* the two terms at the LHS of Eq.(12). The second (Fig. 6) reports the ratio between the surface average mass flux for the absorption of SO_2 on a spherical charged droplet (N) against the case of an uncharged droplet of similar size and exchange area (N_0), for a fixed value of y^*. This allows comparing the effects of droplet charge over the mass transfer coefficient, regardless of its effect on the driving force, *i.e.* on the difference y-y^*.

The last chart (Fig. 7) reports the same ratio as Fig. 6 for a y^* variable with the interfacial solubility, y^*=$m(q)x_0$, so to include in the comparison the effect of droplet charge on the driving force.

This last chart is the more realistic of the three, since it represents the actual comparison between the mass rate of charged and uncharged droplets having the same geometry.

To scan the droplet diameter range, we assume stagnant flow conditions from 100 to 1000 μm, circulating flow conditions from 500 to 2000 μm and oscillating flow conditions from 1500 to 2000 μm. Each flow condition is extended well beyond its theoretical limit (<500 μm for stagnant flow, above 1700 μm for oscillating flow) to better represent intermediate conditions.

Fig. 5 shows that the effect of droplet charge is higher for finer droplets, in the stagnant mass flow conditions, but remains always below 0.2% in all cases. In terms of flow rate, looking at Eq. (12) this means that for y_I=y^*=0, electrophoretic contribution to the overall mass transfer rate are very limited, but for y_I=99% y_0 it increases the mass transfer rate up to 20% with respect to the uncharged conditions:

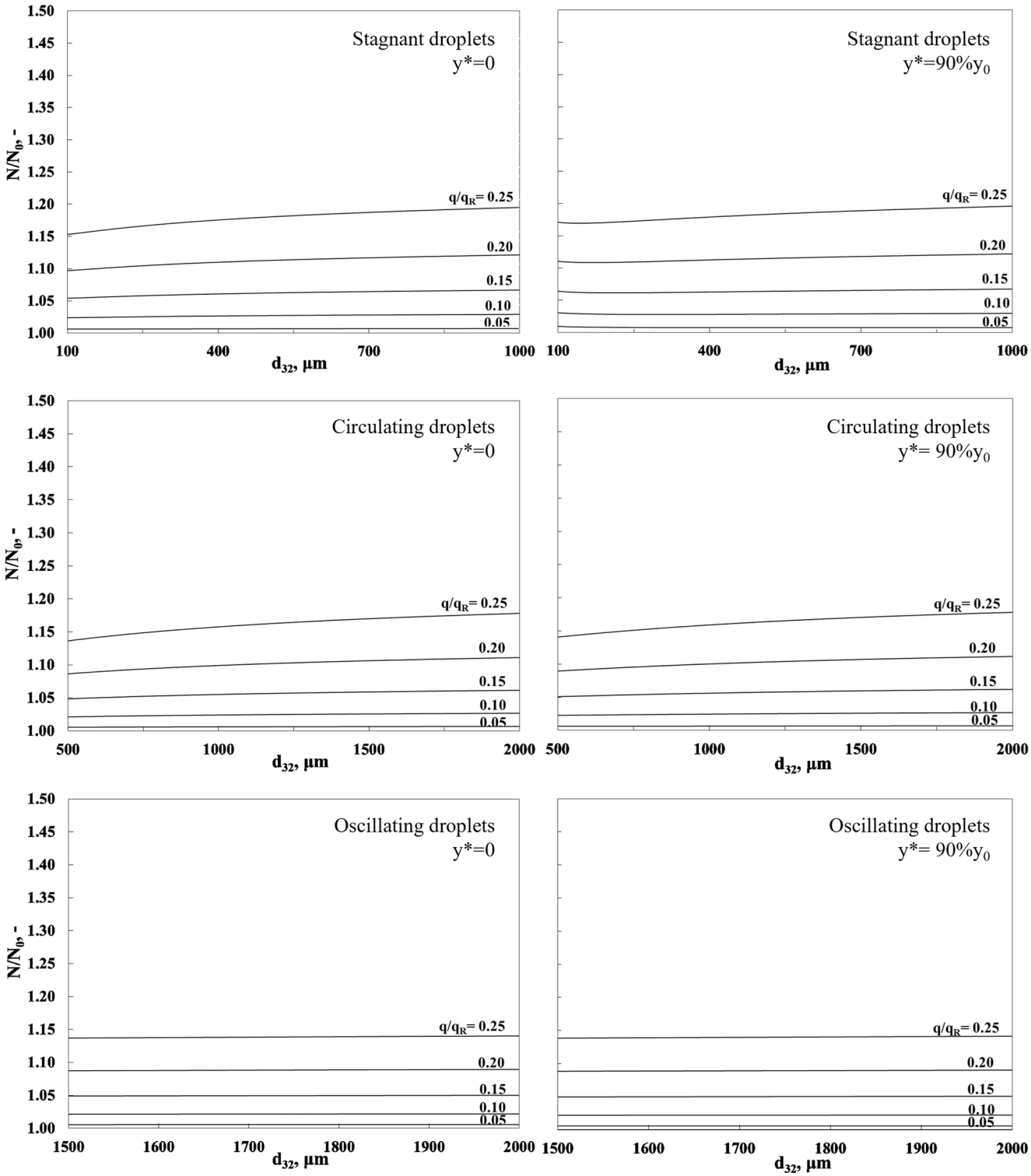

Fig. 6. Ratio between the surface average mass flux for the absorption of SO_2 on the spherical charged droplet (N) against the case of an uncharged droplet of similar size and exchange area (N_0), for y*=0 and y*=90 %y_0 and under stagnant, circulating and oscillating conditions.

Electrophoresis is likely to provide an increasing contribution to mass transfer rate as the solute concentration in the droplet increases. Besides, the low ratio k_e/k_g observed in Fig. 5 also indicates that the interfacial conditions in Eq. (18) mostly depend on the value of $m(q)$.

Fig. 6 shows that by keeping constant the value of y^* (0 and 90% y_0), the mass flux should enhance up to 15% −20% at $q/q_R = 25\%$, with larger effects for stagnant flow conditions. Besides, under stagnant and circulating flow conditions, the flux for charged droplets is slightly increasing with the droplet size, while being constant for oscillating flow.

Fig. 7 indicates that, by including all the effects of droplet charge, either in terms of electrophoresis, mass transfer coefficients and driving force, the electrification gives rise to a substantial increase of the mass flux (and consequently of the mass transfer rate having kept the surface constant in this calculation) up to 35% and 42% for droplets charged up to 25% of the Rayleigh limit respect to their equivalent uncharged

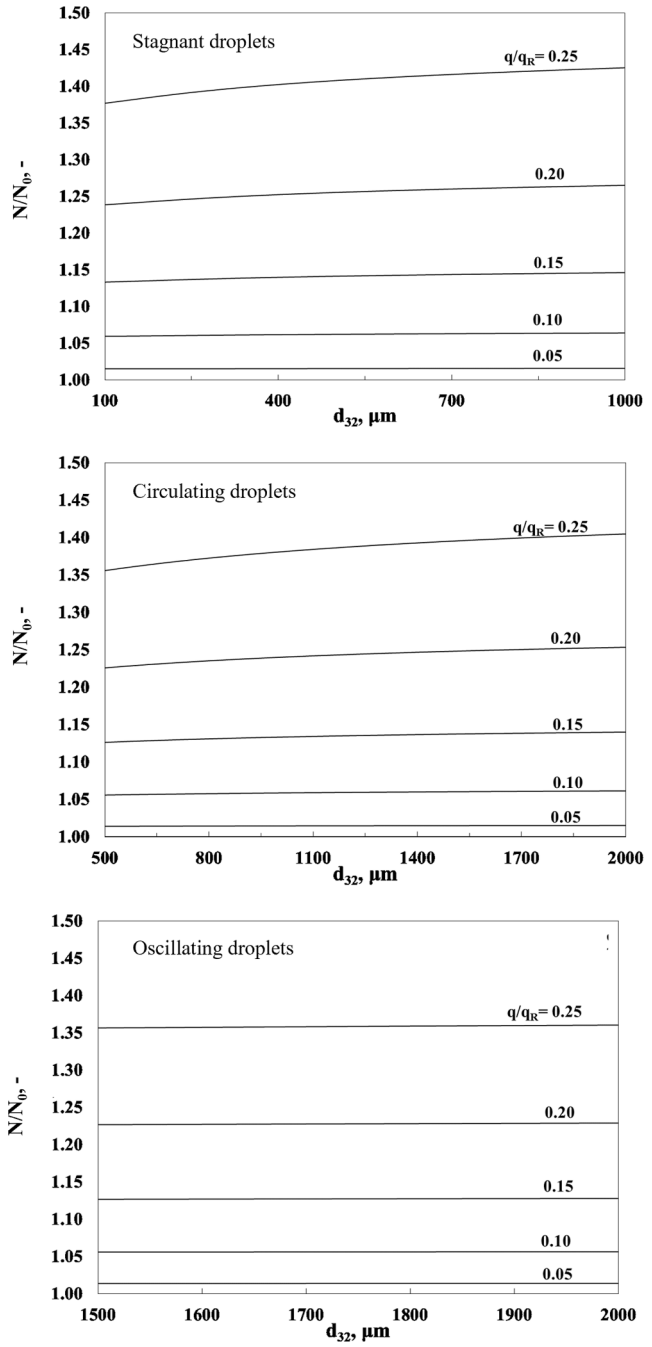

Fig. 7. Ratio between the surface average mass flux for the absorption of SO_2 on the spherical charged droplet (N) against the case of an uncharged droplet of similar size and exchange area (N_0), for $y^*=m(q)x_0$. Droplet models: stagnant (**A**), circulating (**B**) and oscillating (**C**).

conditions. Such a charging level can be achieved with contact charging electrosprays (Carotenuto et al., 2010; Cloupeau and Prunet-Foch, 1989). Increased rate between 5% and 15% can be achieved for droplets charging up to 10–15% of the Rayleigh limit, which are typical of induction and corona charging electrospray (Carotenuto et al., 2010; Hensley et al., 2008).

4. Conclusions

This paper proposes a predictive model for the absorption of trace gases into charged water droplets, which are either present in Nature or produced by electrohydrodynamic atomization. The model incorporates the effects of three main physical phenomena which are likely to be affected by the presence of a net charge over the droplets: i) the onset of electrophoretic attraction occurring between charged droplet and polar molecules or oppositely charged ions; ii) the modification of droplets' morphology following to a reduction of surface tension and iii) the alteration of interfacial solubility.

The mass transfer model was validated against experimental data available for SO_2 absorption in an acidic water solution, for an electrospray operated in dripping mode. The model predictions were highly consistent with the experimental findings, with determination factors up to 99%. This model validation makes it possible to understand how droplet charging alters the absorption rate through electrophoresis and interfacial solubility effects. Besides, it also highlights the importance of assessing correlations for the mass transfer coefficients that better fit the droplets morphology and hydrodynamics, which are significantly altered during electrospraying experiments. In this work, we took advantage of direct optical analyses and physical considerations (Clift et al., 1978; Grace et al., 1976; Kumar and Hartland, 1999; Wegener et al., 2014; Yeh, 2002). On these bases, the more suitable correlations available in the pertinent literature for the mass transfer coefficients in the liquid and the gas films can be selected. As a general rule, we highly recommend verification of the mass transfer coefficient models before proceeding to the evaluation of the mass transfer rate for both uncharged and charged droplets.

Considering the SO_2-air-water system as a reference case study, the model equations have been used to investigate the absorption rate of charged droplets as a function of their size and charge density. The model predicts that the mass transfer rate can be increased up to 42% for droplet charged at 25% of the Rayleigh limit charge, a value that can be reasonably achieved by conventional small-scale contact electrosprays (Carotenuto et al., 2010; Cloupeau and Prunet-Foch, 1989). At droplets charge densities characteristics of large-scale induction or corona spray charging units, *i.e.* within 5–15% the Rayleigh limit charge (Carotenuto et al., 2010; Hensley et al., 2008), a 5–12% improvement can be observed. For the reference case study, an increasing of the droplet charge gives rise to slightly higher values of the surface averaged mass flux for larger droplets. This result mirrors droplets size effects on the mass transfer coefficients, but cannot be considered as a general result since it is also related to the solubility of the absorbed gas: a lower interfacial solubility (*i.e.* higher values of the partition factor) leads to a higher relevance of the liquid side mass transfer rate and a smaller dependence of the surface averaged mass flux on the droplet size.

Considering the contribution of electrophoretic flow to the gas-phase mass transfer, the model predicts higher effects for droplets finer than 500 µm. This result is interesting because it means that in a gas-phase controlled absorption process (*e.g.* for a chemical absorption process with instantaneous reaction at the interface) the electrification provides stronger effects if finer droplets are adopted.

In conclusion, the proposed model gives an accurate description of experiments and provides a theoretical framework to understand the absorption of trace gases into charged droplets. The model also suggests that droplet electrification is a valuable and cost-effective way to improve the mass transfer rate of absorption. Indeed, former experiences indicated that energy consumption for electrospraying of water is within 0.2–0.3 kJ/m^3 (Di Natale et al., 2022) against a pumping cost of at least 98.1 kJ/m^3 required to pump water at 1 bar$_g$. With the potential increase of absorption rate up to within 15–40%, spray electrification provides an appreciable increase of spray towers efficiency with almost no effect on

List of Symbols

A	Droplet surface during fall	m^2
$A(\tau)$	Droplet surface during formation	m^2
C_D	Dimensionless drag coefficient	–
$D\text{-}CMR$	Droplet-to-charge mass ratio	$\mu C \cdot kg^{-1}$
D_g	Gas diffusivity in the gas phase	$m^2 \cdot s^{-1}$
D_l	Gas diffusivity in the liquid phase	$m^2 \cdot s^{-1}$
d_{32}	Sauter mean diameter of the droplet	m
$d(\tau)$	Droplet diameter during formation	m
E	Electric field generated by the droplet close to its surface	V/m
E_a	Interaction energies term between solvent and solute molecules	$kg \cdot m^2 \cdot s^{-2}$
F_e	Force acting between a charged water drop surface and the solute molecule	N
f	droplet frequency	Hz
i	index for the time discretization	-
K	Number of droplets present in the vessel at time t	-
k	Boltzmann constant	$J \cdot K^{-1}$
k_e	Electrophoretic coefficient	$m \cdot s^{-1}$
k_g	Mass transfer coefficient referred to the gas driving force	$m \cdot s^{-1}$
$k_{g,f}$	Gas side mass transfer coefficients during droplet falling	$m \bullet s^{-1}$
$k_{g,p}(\tau)$	Gas side mass transfer coefficients during droplet formation	$m \bullet s^{-1}$
k_g°	Overall mass transfer coefficient referred to the gas-phase driving force	$m \cdot s^{-1}$
k_l	Mass transfer coefficient referred to the liquid driving force	$m \cdot s^{-1}$
m_0	Partition factor for uncharged droplets	$mol \bullet mol^{-1}$
$m(q)$	Partition factor for charged droplets	$mol \bullet mol^{-1}$
N	Surface average mass flux of the solute for charged droplets	$mol \cdot m^{-2} \cdot s^{-1}$
N_0	Surface average mass flux of the solute for uncharged droplets	$mol \cdot m^{-2} \cdot s^{-1}$
n	Total mass of solute in the liquid droplet	mol
$n_{D,i}$	Amount of SO_2 absorbed by a generic droplet during its lifetime	mol
$n_{f,i}(\tau_f)$	Amount of SO_2 absorbed by the falling droplet	mol
$n_{p,i}(\tau_p)$	Amount of SO_2 absorbed by the pendant droplet	mol
N_e	Electric drift flow	$mol \cdot m^{-2} \cdot s^{-1}$
P	Pressure	Pa
P_I	Pressure at the interface	Pa
p	Solute electric dipole moment	C·m
q	Droplet charge at a given potential	C
q_R	Droplet charge at the Rayleigh limit	C
Q	Water flow rate	$L \bullet s^{-1}$
r_M	Solute molecular radius	m
r_s	Absorption rate of SO_2 by sprayed droplets	$mol \cdot s^{-1}$
r_w	Baseline depletion of SO_2 on the closed-loop system wall	$mol \cdot s^{-1}$
R^2	Determination factor	-
Re_g	Reynolds number for the gas around a single droplet	-
$Re_g(\tau)$	Reynolds number for the gas phase during droplet formation	-
RSS	Residual Sum of Squares	$mol^2 \cdot m^{-6}$
Sc_g	Schmidt gas number	-
t	Time variable	s
T	Temperature	K
T_I	Temperature at the interface	K
TSS	Total Sum of Squares	$mol^2 \cdot m^{-6}$
u	gas velocity	$m \bullet s^{-1}$
U	Droplet terminal velocity	$m \bullet s^{-1}$
V	Volume of the vessel	m^3
V_d	Droplet volume during fall	m^3
$V_d(\tau)$	Droplet volume during formation	m^3
v_e	Modulus of the electrical drift velocity	$m \cdot s^{-1}$
x	Gas solute concentration in the liquid phase	$mol \cdot m^{-3}$
x_I	Solute concentration in the liquid phase at the interface	$mol \cdot m^{-3}$
y	Instantaneous gas solute concentration in the gas phase	$mol \cdot m^{-3}$
y_0	Initial gas solute concentration in the gas phase	$mol \cdot m^{-3}$
y^*	gas solute concentration in equilibrium with the solute in the bulk liquid phase	$mol \cdot m^{-3}$
y_I	gas solute concentration in the gas phase at the interface	$mol \cdot m^{-3}$
$y_{i,exp}$	experimental value of the SO_2 concentration in the gas phase at the time t_i	$mol \cdot m^{-3}$
$yi_{,mod}$	modelling value of the SO_2 concentration in the gas phase at the time t_i	$mol \cdot m^{-3}$
y_{avg}	mean value of the SO2 experimental concentration data	$mol \cdot m^{-3}$
Greek symbols		
Δt	Amplitude of each time interval for the solution algorithm	s
ε	Ratio of specific area oscillation to minimum specific area	-
ε_0	Vacuum permittivity	$C^2 \cdot m^{-2} \cdot N^{-1}$
Λ_w°	Baseline scavenging parameter	$m^3 \cdot s^{-1}$
μ	Solute thermal mobility	$N^{-1} \cdot m \cdot s^{-1}$
μ_g	Gas viscosity	$kg \cdot m^{-1} \cdot s^{-1}$
μ_l	Liquid viscosity	$kg \cdot m^{-1} \cdot s^{-1}$
ρ_g	Mass gas density	$kg \cdot m^{-3}$
ρ_l	Mass liquid density	$kg \cdot m^{-3}$
σ	Surface tension for a liquid system	$N \cdot m^{-1}$
σ_0	Surface tension for uncharged water	$N \cdot m^{-1}$
τ	Instant of the droplet's lifetime	s
τ_f	Droplet lifetime	s

(*continued on next page*)

List of Symbols (*continued*)

τ_p	Droplet formation time	s
ω	Frequency of oscillation of liquid droplets	rad·s^{-1}

the operating costs. For this reason, electrified sprays can be used to design new absorbers (and by extension stripping, humidification or evaporation units) and electrification is worthy of further pursuits to exploit its potentiality in sustainable chemical engineering applications.

Declaration of Competing Interest

The authors declare that they have no known competing financial interests or personal relationships that could have appeared to influence the work reported in this paper.

Data availability

Data will be made available on request.

References

Agostinho, L.L.F., Bos, B., Kamau, A., Brouwer, S.P., Fuchs, E.C., Marijnissen, J.C.M., 2018. Simple-jet mode electrosprays with water. Description, characterization and application in a single effect evaporation chamber. J. Aerosol. Sci. 125, 237–250. https://doi.org/10.1016/j.jaerosci.2018.04.010.

Angelo, J.B., Lightfoot, E.N., Howard, D.W., 1966. Generalization of the penetration theory for surface stretch: Application to forming and oscillating drops. AIChE J. 12, 751–760. https://doi.org/10.1002/aic.690120423.

Beattie, J., 2016. The mechanism of spray electrification: the waterfall effect. Atmos. Chem. Phys. 1–9 https://doi.org/10.5194/acp-2015-892.

Bhaga, D., Weber, M.E., 1981. Bubbles in viscous liquids: shapes, wakes and velocities. J. Fluid Mech. 61–85.

Bird, R.B., Stewart, W.E., Lightfoot, E.N., 2007. Transport Phenomena, 2nd ed. John Wiley & Sons.

Boda, S.K., Li, X., Xie, J., 2018. Electrospraying an enabling technology for pharmaceutical and biomedical applications: A review. J. Aerosol. Sci. https://doi.org/10.1016/j.jaerosci.2018.04.002.

Bodnár, E., Grifoll, J., Rosell-Llompart, J., 2018. Polymer solution electrospraying: A tool for engineering particles and films with controlled morphology. J. Aerosol. Sci. 125, 93–118. https://doi.org/10.1016/j.jaerosci.2018.04.012.

Borra, J.P., 2018. Review on water electro-sprays and applications of charged drops with focus on the corona-assisted cone-jet mode for High Efficiency Air Filtration by wet electro-scrubbing of aerosols. J. Aerosol. Sci. 125, 208–236. https://doi.org/10.1016/j.jaerosci.2018.04.005.

Brunson, R.J., Wellek, R.M., 1970. Mass transfer within oscillating liquid droplets. Can. J. Chem. Eng. 48, 267–274. https://doi.org/10.1002/cjce.5450480308.

Burgo, T.A.L., Galembeck, F., 2016. Electrified water: Liquid, vapor and aerosol. J. Braz. Chem. Soc. 27, 229–238. https://doi.org/10.5935/0103-5053.20150303.

Byun, Y.-C., Jung, J.-Y., Hwang, J., 1998. Application of electrostatic spraying to reduce SO2 emission in a laboratory-scale spray drying absorber. J. AemsoI. Sci.

Carotenuto, C., Di Natale, F., Lancia, A., 2010. Wet electrostatic scrubbers for the abatement of submicronic particulate. Chem. Eng. J. 165, 35–45. https://doi.org/10.1016/j.cej.2010.08.049.

Castillo, J.L., Martin, S., Rodriguez-Perez, D., Higuera, F.J., Garcia-Ybarra, P.L., 2018. Nanostructured porous coatings via electrospray atomization and deposition of nanoparticle suspensions. J. Aerosol. Sci. 125, 148–163. https://doi.org/10.1016/j.jaerosci.2018.03.004.

Choi, D., Kim, D.W., Yoo, D., Cha, K.J., La, M., Kim, D.S., 2017. Spontaneous occurrence of liquid-solid contact electrification in nature: Toward a robust triboelectric nanogenerator inspired by the natural lotus leaf. Nano Energy 36, 250–259. https://doi.org/10.1016/j.nanoen.2017.04.026.

Clift (Roland), R., Grace, J.R., Weber, M.E., 1978. Bubbles, drops, and particles. Academic Press.

Cloupeau, M., Prunet-Foch, B., 1989. Electrostatic spraying of liquids in cone-jet mode. J. Electrostat. 22, 135–159.

Conde, J.J., Ferreira-Aparicio, P., Chaparro, A.M., 2021. Electrospray deposition: A breakthrough technique for proton exchange membrane fuel cell catalyst layer fabrication. ACS Appl. Energy Mater. https://doi.org/10.1021/acsaem.1c01445.

Consta, S., 2022. Atomistic modeling of jet formation in charged droplets. J. Phys. Chem. B 126, 8350–8357. https://doi.org/10.1021/acs.jpcb.2c05849.

Couper, J.R., 2010. Chemical process equipment: selection and design. Butterworth-Heinemann.

Cui, H., Li, N., Peng, J., Cheng, J., Zhang, N., Wu, Z., 2017. Modeling the particle scavenging and thermal efficiencies of a heat absorbing scrubber. Build. Environ. 111, 218–227. https://doi.org/10.1016/j.buildenv.2016.11.006.

D'Addio, L., Di Natale, F., Carotenuto, C., Balachandran, W., Lancia, A., 2013. A lab-scale system to study submicron particles removal in wet electrostatic scrubbers. Chem. Eng. Sci. 97, 176–185. https://doi.org/10.1016/j.ces.2013.04.006.

D'Addio, L., Carotenuto, C., Balachandran, W., Lancia, A., Di Natale, F., 2014. Experimental analysis on the capture of submicron particles (PM0.5) by wet electrostatic scrubbing. Chem. Eng. Sci. 106, 222–230. https://doi.org/10.1016/j.ces.2013.11.044.

Danckwerts, P., v., Lannus, A.,, 1970. Gas-liquid reactions. J. Electrochem. Soc. 117, 369C–370C.

Davies, J.T., 1972. Turbulence phenomena at free surfaces. AIChE J 18, 169–173. https://doi.org/10.1016/b978-0-12-206070-0.x5001-9.

Di Natale, F., Carotenuto, C., D'Addio, L., Jaworek, A., Krupa, A., Szudyga, M., Lancia, A., 2015. Capture of fine and ultrafine particles in a wet electrostatic scrubber. J. Environ. Chem. Eng. 3, 349–356. https://doi.org/10.1016/j.jece.2014.11.007.

Di Natale, F., Carotenuto, C., Lancia, A., 2016. Enhanced SO_2 removal by using charged water droplets. Chem. Eng. Trans. 52, 505–510. https://doi.org/10.3303/CET1652085.

Di Natale, F., Carotenuto, C., Manna, L., Lancia, A., 2018. Chemi-electro-hydrodynamic of sulphur dioxide absorption by electrified water sprays. Chem. Eng. Trans. 69, 685–690. https://doi.org/10.3303/CET1869115.

Di Natale, F., Carotenuto, C., Caserta, S., Troiano, M., Manna, L., Lancia, A., 2019. Experimental evidences on the chemi-electro-hydrodynamic absorption of sulphur dioxide in electrified water sprays. Chem. Eng. Res. Des. 146, 249–262. https://doi.org/10.1016/j.cherd.2019.04.006.

Di Natale, F., Carotenuto, C., Parisi, A., Lancia, A., 2020. Absorption of sulphur dioxide by electrosprayed droplets. Can. J. Chem. Eng. 98, 1989–1997. https://doi.org/10.1002/cjce.23821.

Di Natale, F., Carotenuto, C., Parisi, A., Flagiello, D., Lancia, A., 2022. Wet electrostatic scrubbing for flue gas treatment. Fuel 325. https://doi.org/10.1016/j.fuel.2022.124888.

Dou, B., Pan, W., Jin, Q., Wang, W., Li, Y., 2009. Prediction of SO2 removal efficiency for wet Flue Gas Desulfurization. Energy Convers. Manag. 50, 2547–2553. https://doi.org/10.1016/j.enconman.2009.06.012.

Dreyer, W., Guhlke, C., Landstorfer, M., Müller, R., 2018. New insights on the interfacial tension of electrochemical interfaces and the Lippmann equation. Eur. J. Appl. Math. 29, 708–753. https://doi.org/10.1017/S0956792517000341.

Eggers, J., Villermaux, E., 2008. Physics of liquid jets. Rep. Prog. Phys. 71 https://doi.org/10.1088/0034-4885/71/3/036601.

Elhajj, J., Al-Hindi, M., Azizi, F., 2014. A review of the absorption and desorption processes of carbon dioxide in water systems. Ind. Eng. Chem. Res. 53, 2–22. https://doi.org/10.1021/ie403245p.

Flagiello, D., Erto, A., Lancia, A., di Natale, F., 2018. Experimental and modelling analysis of seawater scrubbers for sulphur dioxide removal from flue-gas. Fuel 214, 254–263. https://doi.org/10.1016/j.fuel.2017.10.098.

Flagiello, D., Parisi, A., Lancia, A., Carotenuto, C., Erto, A., di Natale, F., 2019. Seawater desulphurization scrubbing in spray and packed columns for a 4.35 MW marine diesel engine. Chem. Eng. Res. Des. 148, 56–67. https://doi.org/10.1016/j.cherd.2019.05.057.

Flagiello, D., Erto, A., Lancia, A., Di Natale, F., 2020. Dataset of wet desulphurization scrubbing in a column packed with Mellapak 250. X. Data in Brief, 33, 106383.

Funakawa, T., Balachandran, W., 2006. Molecular dynamics simulation of charged liquid - Vapor interface instability. In: 10th International Conference on Liquid Atomization and Spray Systems, ICLASS 2006.

Galembeck, F., Burgo, T.A.L., 2017. Chemical electrostatics: New ideas on electrostatic charging: Mechanisms and consequences. Chem. Electrost.: New Ideas on Electrostatic Charging: Mechanisms and Consequences. https://doi.org/10.1007/978-3-319-52374-3.

Ganán-Calvo, A.M., 2004. On the general scaling theory for electrospraying. J. Fluid Mech. 203–212 https://doi.org/10.1017/S0022112004008870.

Garner, F.H., Tayeban, M., 1960. Continuous phase mass transfer coefficients in oscillating drops. Anales de la Real Sociedad Española de Física y Química 56, 479.

Giberti, F., Hassanali, A.A., 2017. The excess proton at the air-water interface: The role of instantaneous liquid interfaces. J. Chem. Phys. 146 https://doi.org/10.1063/1.4986082.

Goldman, S., 1985. Theories of solubilities of non-electrolytes. Pure Appl. Chem. 57, 273–282.

Gong, P., Li, X., 2021. Simultaneous removal of NOx and SO2 from simulated marine ship flue gas in a novel wet scrubbing system based on divided diaphragm seawater electrolysis technology: Efficiency optimization and economic assessment. Water Sci. Technol. 83, 1230–1241. https://doi.org/10.2166/wst.2021.053.

Grace, J.R., Wairegi, T., Nguyen, T.H., 1976. Shapes and velocities of single drops and bubbles moving freely through immiscible liquids. Transactions of the American Institute of Chemical Engineers Volume 54.

Green, D.W., Perry, R.H., 2018. Perry's Chemical Engineers' Handbook.

Griffith, R.M., 1960. Mass transfer from drops and bubbles. Chem. Eng. Sci. 12, 198–213. https://doi.org/10.1016/0009-2509(60)85006-3.

Handlos, A.E., Baron, T., 1957. Mass and heat transfer from drops in liquid-liquid extraction. AIChE J 3, 127–136. https://doi.org/10.1002/aic.690030121.

Hassan, M.E., Janda, M., Machala, Z., 2021. Transport of gaseous hydrogen peroxide and ozone into bulk water vs. Electrosprayed aerosol. Water (Switzerland) 13. https://doi.org/10.3390/w13020182.

Hensley, J.L., Feng, X., Bryan, J.E., 2008. Induction charging nozzle for flat fan sprays. J. Electrostat. 66, 300–311. https://doi.org/10.1016/j.elstat.2007.08.012.
Hohman, M.M., Shin, M., Rutledge, G., Brenner, M.P., 2001a. Electrospinning and electrically forced jets. II. Applications. Phys. Fluids 13, 2221–2236. https://doi.org/10.1063/1.1384013.
Hohman, M.M., Shin, M., Rutledge, G., Brenner, M.P., 2001b. Electrospinning and electrically forced jets. I. Stability theory. Phys. Fluids 13, 2201–2220. https://doi.org/10.1063/1.1383791.
Horikoshi, S., Serpone, N., 2017. In-liquid plasma: A novel tool in the fabrication of nanomaterials and in the treatment of wastewaters. RSC Adv. 7, 47196–47218. https://doi.org/10.1039/c7ra09600c.
Hu, B., Yao, Z.P., 2018. Detection of native proteins using solid-substrate electrospray ionization mass spectrometry with nonpolar solvents. Anal. Chim. Acta 1004, 51–57. https://doi.org/10.1016/j.aca.2017.11.079.
Hughmark, G.A., 1967. Liquid-liquid spray column drop size, holdup, and continuous phase mass transfer. Ind. Eng. Chem. Fundam. 6, 408–413. https://doi.org/10.1021/i160023a014.
Jain, C.D., Madhavan, B.L., Ratnam, M.V., 2019. Source apportionment of rainwater chemical composition to investigate the transport of lower atmospheric pollutants to the UTLS region. Environ. Pollut. 248, 166–174. https://doi.org/10.1016/j.envpol.2019.02.007.
Jaworek, A., Krupa, A., 1999. Classification of the modes of EHD Spraying. J. Aerosol. Sci. 30, 873–893.
Jiang, K., Yu, H., Chen, L., Fang, M., Azzi, M., Cottrell, A., Li, K., 2020. An advanced, ammonia-based combined NOx/SOx/CO2 emission control process towards a low-cost, clean coal technology. Appl. Energy 260. https://doi.org/10.1016/j.apenergy.2019.114316.
Kallay, N., Preočanin, T., Selmani, A., Kovačević, D., Lützenkirchen, J., Nakahara, H., Shibata, O., 2015. Thermodynamic model of charging the gas/water interface. J. Phys. Chem. C 119, 997–1007. https://doi.org/10.1021/jp507477u.
Kim, Y., Jung, S., Kim, S., Choi, S.T., Kim, M., Lee, H., 2020. Heat transfer performance of water-based electrospray cooling. Int. Commun. Heat Mass Transfer 118. https://doi.org/10.1016/j.icheatmasstransfer.2020.104861.
Kishimoto, T., Kadota, K., Furukawa, R., Tozuka, Y., Shimosaka, A., Shirakawa, Y., 2017. Nozzleless electrostatic atomization process for crystallization via liquid-liquid interfaces. J. Chem. Eng. Jpn. 50, 367–375. https://doi.org/10.1252/jcej.16we236.
Klee, A.J., Treybal, R.E., 1956. Rate of rise or fall of liquid drops. AIChE J.
Krupa, A., Jaworek, A., Sobczyk, A.T., Marchewicz, A., Szudyga, M., Antes, T., 2013. Charged spray generation for gas cleaning applications. J. Electrostat. 71, 260–264. https://doi.org/10.1016/j.elstat.2012.11.022.
Kumar, A., Hartland, S., 1999. Correlations for prediction of mass transfer coefficients in single drop systems and liquid-liquid extraction columns. Chem. Eng. Res. Des. 77, 372–384. https://doi.org/10.1205/026387699526359.
Kwan, V., Consta, S., 2020. Bridging electrostatic properties between nanoscopic and microscopic highly charged droplets. Chem. Phys. Lett. 746 https://doi.org/10.1016/j.cplett.2020.137238.
Kwan, V., Consta, S., 2021. Molecular characterization of the surface excess charge layer in droplets. J. Am. Soc. Mass Spectrom. 32, 33–45. https://doi.org/10.1021/jasms.0c00053.
Lamb, H., 1975. Hydrodynamics. Sundics of the Cambridge University Press.
Láng, G.G., 2020. Some remarks to the derivation of the "generalized Lippmann equation". J. Solid State Electrochem. 24, 3039–3047. https://doi.org/10.1007/s10008-020-04745-5/Published.
Levenspiel, O., 1999. Chemical Reactor Engineering, 3rd ed. John Wiley & Sons.
Li, Y., Wang, Z., Kong, Q., Li, B., Wang, H., 2022. Sulfur dioxide absorption by charged droplets in electrohydrodynamic atomization. Int. Commun. Heat Mass Transfer 137. https://doi.org/10.1016/j.icheatmasstransfer.2022.106275.
Lippmann, G., 1875. Relations entre les phénomènes éelectrique et capillaires. Ann. Chim. Phys.
Lochiel, A.C., Calderbank, P.H., 1964. Mass transfer in the continuous phase around axisymmetric bodies of revolution. Chem. Eng. Sci. 19, 471–484. https://doi.org/10.1016/0009-2509(64)85074-0.
Malevanets, A., Consta, S., 2013. Variation of droplet acidity during evaporation. J. Chem. Phys. 138 https://doi.org/10.1063/1.4804303.
Manna, L., Carotenuto, C., Nigro, R., Lancia, A., di Natale, F., 2017. Primary atomization of electrified water sprays. Can. J. Chem. Eng. 95, 1781–1788. https://doi.org/10.1002/cjce.22841.
Marichev, V.A., 2010. General thermodynamic equations for the surface tension of liquids and solids. Surf. Sci. 604, 458–463. https://doi.org/10.1016/j.susc.2009.12.020.
Martin, S., Garcia-Ybarra, P.L., Castillo, J.L., 2017. Long-term operation of a proton exchange membrane fuel cell without external humidification. Appl. Energy 205, 1012–1020. https://doi.org/10.1016/j.apenergy.2017.08.157.
Matito-Martos, I., Martin-Calvo, A., Gutiérrez-Sevillano, J.J., Haranczyk, M., Doblare, M., Parra, J.B., Ania, C.O., Calero, S., 2014. Zeolite screening for the separation of gas mixtures containing SO2, CO2 and CO. PCCP 16, 19884–19893. https://doi.org/10.1039/c4cp00109e.
Matteson, M.J., Giardina, P.J., 1974. Mass transfer of sulfur dioxide to growing droplets role of surface electrical properties. Environ. Sci. Technol. 8, 50–55.
Matteson, M.J., Stringer, H.L., Busbee, W.L., 1972. Corona discharge oxidation of sulfur dioxide. Curr. Res. 6, 895–901.
Matsuda, M., 1980. First Order Algebraic Differential Equations. A Differential Algebraic Approach.
Michaelides, E.E., Crowe, C.T., Schwarzkopf, J.D., 2017. Multiphase flow handbook. Second Edition.
Ohshima, H., Furusawa, K., 1998. Electrical phenomena at interfaces. Fundamentals, measurements, and applications. Second Edition, Revised and Expandes.
Ovchinnikova, K., Pollack, G.H., 2009. Can water store charge? Langmuir 25, 542–547. https://doi.org/10.1021/la802430k.
Parmentier, D., Rybałtowska, A., van Smeden, J., Kroon, M.C., Marijnissen, J.C.M., Lemos, L., 2016. Applying electrohydrodynamic atomization to enhance mass transfer of metal salts from an aqueous phase towards ionic liquids. J. Electrostat. 80, 1–7. https://doi.org/10.1016/j.elstat.2015.11.007.
Pruppacher, H.R., Klett, J.D., 2010. Microphysics of Clouds and Precipitation -Part of the Atmospheric and Oceanographic Sciences Library Book Series (ATSL, volume 18). Springer, Dordrecht Heidelberg London New York https://doi.org/10.1007/978-0-306-48100-0.
Raizer, Y.P., 1991. Gas Discharge Physics, First ed. Springer, Moscow.
Rayleigh, L., 1882. On the Equilibrium of Liquid Conducting Masses Charged with Electricity. The London, Edinburgh, and Dublin Philosophical Magazine and Journal of Science 14, 184–186. https://doi.org/10.1017/cbo9780511703973.013.
Reznikov, M., Salazar, M., Rivera-Sustache, M., Lopez, M., 2003. Electrically enhanced harvesting of water vapor from the air ionic thermodiffusion view project electrically enhanced nucleation and phase change of water view project electrically enhanced harvesting of water vapor from the air.
Rose, P.M., Kintner, R.C., 1966. Mass transfer from large oscillating drops. AIChE J 12, 530–534. https://doi.org/10.1002/aic.690120325.
Rosell-Llompart, J., Grifoll, J., Loscertales, I.G., 2018. Electrosprays in the cone-jet mode: From Taylor cone formation to spray development. J. Aerosol. Sci. 125, 2–31. https://doi.org/10.1016/j.jaerosci.2018.04.008.
Saboni, A., Alexandrova, S., 2001. Sulfur dioxide absorption and desorption by water drops. Chem. Eng. J. 84, 577–580. https://doi.org/10.1016/S1385-8947(01)00172-3.
Salazar, M., Minakata, K., Reznikov, M., 2015. Electrically enhanced condensation II: Effects of the electrospray. IEEE Trans. Ind. Appl. 51, 1146–1152. https://doi.org/10.1109/TIA.2014.2344508.
Santos, L.P., Ducati, T.R.D., Balestrin, L.B.S., Galembeck, F., 2011. Water with excess electric charge. J. Phys. Chem. C 115, 11226–11232. https://doi.org/10.1021/jp202652q.
Schroeder, R.R., Kintner, R.C., 1965. Oscillations of drops falling in a liquid field. AIChE J 11, 5–8. https://doi.org/10.1002/aic.690110105.
Seinfeld, J.H., Pandis, S.N., 1998. Atmospheric Chemistry and Physics, from Air Pollution to Climate Change. John Wiley & Sons Inc, New York https://doi.org/10.1063/1.882420.
Shamay, E.S., Johnson, K.E., Richmond, G.L., 2011. Dancing on water: The choreography of sulfur dioxide adsorption to aqueous surfaces. J. Phys. Chem. C 115, 25304–25314. https://doi.org/10.1021/jp2064326.
Sharif, H.M.A., Mahmood, N., Wang, S., Hussain, I., Hou, Y.N., Yang, L.H., Zhao, X., Yang, B., 2021. Recent advances in hybrid wet scrubbing techniques for NOx and SO2 removal: State of the art and future research. Chemosphere. https://doi.org/10.1016/j.chemosphere.2021.129695.
Shrimpton, J., 2009. Charge Injection Systems. Springer, Berlin Heidelberg, Berlin, Heidelberg https://doi.org/10.1007/978-3-642-00294-6.
Sinha, A.P., De, P., 2012. Mass Transfer Principles and Operations. https://doi.org/10.1017/CBO9781107415324.004.
Sinnott, R., Towler, G., 2019. Chemical Engineering Design. Coulson and Richardson's Chemical Engineering Series. Sixth Edition, Chemical Engineering Design: SI Edition. Elsevier. https://doi.org/10.1016/B978-0-08-102599-4.09980-X.
Sisskind, B., Kasarnowsky, I., 1933. Untersuchunger uber die Loslichkeit der Gase. Zeitschrift fur anorgainische und allgemeine. Chemie.
Thaokar, R.M., Deshmukh, S.D., 2010. Rayleigh instability of charged drops and vesicles in the presence of counterions. Phys. Fluids 22, 7–11. https://doi.org/10.1063/1.3361158.
Tinsley, B.A., Rohrbaugh, R.P., Hei, M., Beard, K.V., 2000. Effects of image charges on the scavenging of aerosol particles by cloud droplets and on droplet charging and possible ice nucleation processes. J. Atmos. Sci. 57, 2118–2134. https://doi.org/10.1175/1520-0469(2000)057<2118:EOICOT>2.0.CO;2.
Tinsley, B., Zhou, L., Plemmons, S., 2006. Changes in scavenging of particles by droplets due to weak electrification in clouds. Atmos. Res. 79, 266–295. https://doi.org/10.1016/j.atmosres.2005.06.004.
Uchigasaki, K., Asano, K., Sugawara, M., Takamatsu, T., 1967. Absorption of Gas in Liquid with Corona Discharge. Science reports of the Research Institutes.
Uhlig, H.H., 1937. The solubilities of gases and surface tension. J. Phys. Chem. 41, 1215–1225.
Vácha, R., Buch, V., Milet, A., Devlin, J.P., Jungwirth, P., 2007. Autoionization at the surface of neat water: is the top layer pH neutral, basic, or acidic? Phys. Chem. Chem. Phys. 9, 4736. https://doi.org/10.1039/b704491g.
Valluri, S., Kawatra, S.K., 2021. Simultaneous removal of CO2, NOx and SOx using single stage absorption column. J. Environ. Sci. (China) 103, 279–287. https://doi.org/10.1016/j.jes.2020.11.006.
Vasishtha, N., Someshwar, A.V., 1988. Absorption characteristics of sulfure dioxide in water in the presence of a corona discharge. Ind. Eng. Chem. Res. 27, 241.
Wang, Z., 2013. Experimental investigation on wet flue gas desulfurization with electrostatically assisted twin fluid atomization. Environ. Eng. Manag. J. 12.
Wang, Z.W., Guo, J., Zeng, H.C., Ge, C.L., Yu, J., 2007. Sulphur dioxide (SO2) electrotransfer in electric field generated by corona discharge. Fuel Process. Technol. 88, 471–475. https://doi.org/10.1016/j.fuproc.2006.12.004.
Wang, Z., Luo, T., 2011. Model and Simulation on SO2 Removal with electrostatic spray. 5th International Conference on Bioinformatics and Biomedical Engineering, ICBBE 2022. IEEE, Wuhan, Hubei, China.

Wegener, M., Paul, N., Kraume, M., 2014. Fluid dynamics and mass transfer at single droplets in liquid/liquid systems. Int. J. Heat Mass Transf. 71, 475–495. https://doi.org/10.1016/j.ijheatmasstransfer.2013.12.024.

Wei, H., Vejerano, E.P., Leng, W., Huang, Q., Willner, M.R., Marr, L.C., Vikesland, P.J., 2018. Aerosol microdroplets exhibit a stable pH gradient. Proc. Natl. Acad. Sci. U. S. A. 115, 7272–7277. https://doi.org/10.1073/pnas.1720488115.

Whitman, W.G., 1962. A preliminary experimental confirmation of the two-film theory of gas absorption- it seems to explain satisfactority the well-recognized differences of absorption rate for varying concentrations. J. Heat Mass Transfer 5, 429–433.

Yamaguchi, M., Fujimoto, T., Katayama, T., 1975. Experimental studies of mass transfer rate in the dispersed phase and moving behavior for single oscillating drops in liquid-liquid systems. J. Chem. Eng. Jpn. 8, 361–366. https://doi.org/10.1252/jcej.8.361.

Yeh, N.K., 2002. Liquid Phase Mass Transfer in Spray Contactors. The University of Texas, Austin.

Yu, X., Li, D., Li, D., Zhang, G., Zhou, H., Li, S., Song, W., Zhang, Y., Bi, X., Yu, J., Wang, X., 2020. Enhanced wet deposition of water-soluble organic nitrogen during the harvest season: influence of biomass burning and in-cloud scavenging. J. Geophys. Res. Atmos. 125, 1–13. https://doi.org/10.1029/2020JD032699.

Zarzycki, R., Chacuk, A., 1993. Absorption Fundamentals & Applications. Pergamon Press Ltd https://doi.org/10.1016/B978-0-08-040262-8.50001-0.

Zhou, J., Wang, H., 2020. Study on efficient removal of SOx and NOx from marine exhaust gas by wet scrubbing method using urea peroxide solution. Chem. Eng. J. 390 https://doi.org/10.1016/j.cej.2020.124567.